





Quantum dynamical signatures of non-Hermitian boundary modes

Fan Yang , Maria Zelenayova , Paolo Mognini , and Emil J. Bergholtz 

Department of Physics, Stockholm University, AlbaNova University Center, 10691 Stockholm, Sweden

(Dated: June 23, 2025)

The non-Hermitian bulk-boundary correspondence features an interplay between the non-Hermitian skin effect and anomalous boundary-mode behavior. Whereas the skin effect is known to manifest itself in quantum dynamics in the form of chiral damping, it has remained less clear what impact the boundary modes may have. Here we derive experimentally accessible signatures of the boundary modes. We also establish clear criteria, based on the effective generalized Brillouin zone, that determine when bulk and boundary effects can be dynamically discerned using the Liouvillian separation gap. This leads to telltale signatures in both stable regimes – where particle number remains finite – and in the unstable regimes – where a macroscopic boundary mode population occurs.

Non-Hermitian (NH) systems have opened up a new paradigm for realizing novel topological phases of matter beyond the conventional Hermitian picture [1, 2]. Two of the most striking features characterizing such systems are the non-Hermitian skin effect (NHSE) and the breakdown of conventional bulk-boundary correspondence (BBC) [3–7]. The NHSE refers to the extensive accumulation of eigenstates near system boundaries. This phenomenon is intimately connected with an extreme spectral sensitivity to boundary conditions, widely observed across various experimental platforms [8–15]. This anomalous boundary sensitivity is connected to non-Bloch band theory [5, 6, 16, 17], which links the topology of the complex bulk spectrum to boundary modes in a way that departs from conventional topological band theory [18, 19]. Besides underpinning deep theoretical implications for the topological classification of dissipative systems, NH phenomenology also offers exciting prospects for technological applications. These include unidirectional single-mode lasing [20], topological light funneling [21], nonreciprocal state pumping [22], and enhanced sensing [23–26].

This new paradigm naturally manifests in the framework of open quantum systems, which have dissipation and decoherence as essential features. Such systems are described by the action of an inherently non-Hermitian Liouvillian superoperator – encoding both coherent and dissipative dynamics – on the density matrix of the system. The NHSE reappears in this broader context as the *Liouvillian skin effect*, with recent studies revealing its presence in both non-interacting [27–30] and interacting [31–35] settings. In contrast, the precise role of boundary modes linked to the NH BBC has remained elusive [36]. The extent to which the anomalous boundary modes can be dynamically isolated from bulk modes, or even detectable at all in realistic dissipative settings, remains unclear.

In this work, we resolve this question by providing exact solutions to a class of quadratic bosonic Lindbladians (QBLs), where sublattice dissipation can be engineered to enhance boundary contributions [37–41]. Compared

with open fermions [42–47], the dynamics of open bosonic systems remains significantly less explored, with previous works focusing on steady-state properties [48, 49]. One of the challenges lies in the unbounded bosonic Liouville space [50], leading to dynamical instabilities in finite-size systems with open boundaries [51]. While such instabilities pose technical challenges, they also open the door to unique bosonic phenomena such as directional amplification [52] and non-Hermitian lasing [53, 54].

Our results offer a quantitative analysis of this landscape. We show that when the system exhibits a positive *Liouvillian separation gap* – defined from the real spectral gap isolating a boundary mode from all other bulk modes – the boundary mode becomes dynamically dominant. Such separation can be achieved by tuning sublattice dissipation, as observed numerically in Ref. [36]. On the other hand, the instability of the non-equilibrium system is characterized by a negative *Liouvillian gap* [50, 51] – defined from the minimum of the real spectrum – and occurs once global gain surpasses loss. Moreover, akin to quadratic fermionic Lindbladians [55], we find that the topology of QBLs is not connected to steady states, but encoded in a NH damping matrix which shapes skin modes of different orders during relaxations. We trace their BBC back to a *polarization drift* – the difference in long-time polarization before and after elevating/isolating NH boundary mode from the bulk using sublattice dissipation (Fig. 1).

Our work provides a new theoretical lens on the separability of NH bulk and boundary modes in open quantum matter, and should inform the design of future NH photonic, atomic, or superconducting platforms where boundary-mode engineering is critical.

The dynamics of an open bosonic system can be described by the Lindblad master equation [56, 57]:

$$\frac{d\rho}{dt} = \hat{\mathcal{L}}\rho := -i[\mathcal{H}, \rho] + \sum_{\mu} (L_{\mu}\rho L_{\mu}^{\dagger} - \frac{1}{2}\{L_{\mu}^{\dagger}L_{\mu}, \rho\}), \quad (1)$$

where ρ is the density matrix. We consider a lattice of n sites with a tight-binding Hamiltonian $\mathcal{H} = \underline{b}^{\dagger} H \underline{b}$ and bosonic creation (annihilation) operators b_j^{\dagger}

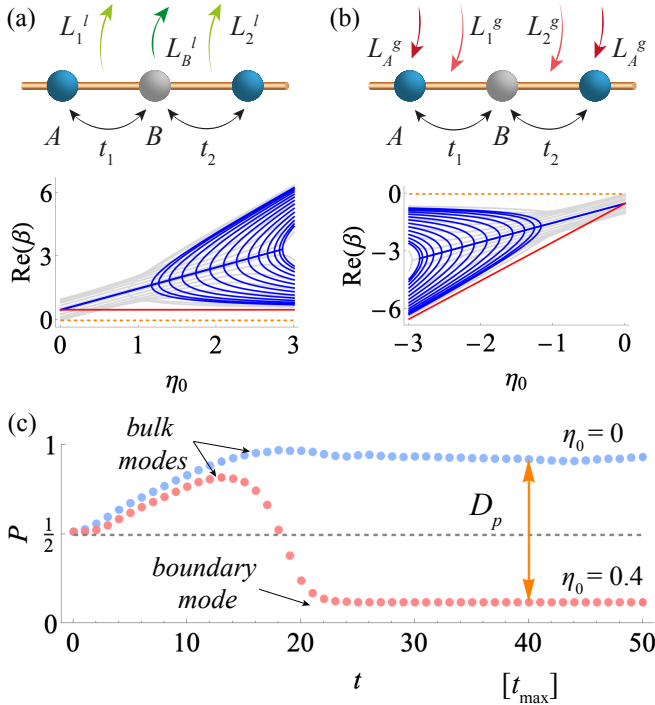


FIG. 1. **Distillation vs. Amplification: two scenarios to isolate NH boundary modes in bosonic Lindbladians.** (a) Distillation scheme with loss on bonds and sublattice B. (b) Amplification scheme with gain on bonds and sublattice A. The bottom panels depict the real part of the rapidity spectrum (OBC), shown as a function of sublattice dissipation η_0 for $N_{\text{tot}} = 2N - 1 = 29$ sites at fixed (a) $t_1 = 1, t_2 = 2, \eta_1 = 0.5, \eta_2 = 0$ and (b) $t_1 = -1, t_2 = 2, \eta_1 = -0.5, \eta_2 = 0$. The Liouvillian gap between boundary (red) and bulk (blue) modes is enlarged by increasing $|\eta_0|$. The PBC rapidity spectrum is shown in gray. (c) Illustration of polarization drift D_p as a change in long-time polarization when increasing η_0 from 0 to 0.4 in the distillation scenario (a). The bulk and boundary modes exhibit localization lengths $r_{\xi, \text{bulk}} = |r|^{-1} \simeq 1.73$ ($P \rightarrow 1$) and $r_{\xi, \text{boundary}} = |r_L| = 0.75$ ($P \rightarrow 0$), respectively.

(b_j). Dissipation is modeled via linear jump operators $L_\mu^l = l_\mu \cdot \underline{b}$ (loss) and $L_\mu^g = g_\mu \cdot \underline{b}^\dagger$ (gain), where $\underline{x} = (x_1, x_2, \dots, x_n)^T$. Using third quantization for bosons [50], the eigenvalues (also called *rapidities*) and eigenvectors of the Liouvillian can be directly obtained [58] from the damping matrix $X = iH^T + \frac{1}{2}[(M^l)^T - M^g]$ with $M^l = \sum_\mu l_\mu^\dagger l_\mu$ and $M^g = \sum_\mu g_\mu^\dagger g_\mu$. Physical observables are fully determined by the two-point correlator $C_{jk}(t) = \text{Tr}[\rho(t)b_j^\dagger b_k]$, whose evolution obeys $\partial_t C(t) = -X^\dagger C(t) - C(t)X + M^g$. Deviations $\tilde{C}(t) = C(t) - C_s$ from the stationary covariance matrix C_s – satisfying $\partial_t C_s(t) = 0$ – have a closed-form solution in terms of the biorthogonal eigenvalue decomposition [59] of $X = \sum_m \beta_m |\psi_{R,m}\rangle \langle \psi_{L,m}|$ with $\langle \psi_{L,m} | \psi_{R,m'} \rangle = \delta_{m,m'}$:

$$\tilde{C}(t) = \sum_{m,m'} e^{-(\beta_m^* + \beta_{m'})t} |\psi_{L,m}\rangle I_{m,m'} \langle \psi_{L,m'}|. \quad (2)$$

Here, $I_{m,m'} = \langle \psi_{R,m} | \tilde{C}(0) | \psi_{R,m'} \rangle$. The rapidities β_m encompass both a boundary mode (which we label with $m = 0$) and bulk modes ($m \neq 0$). The decay (or growth) rate of each mode is determined by the real part of its rapidity β_m . Globally, the stability of QBLs can be quantified with the *Liouvillian gap* $\Delta \equiv 2 \min_m \text{Re}[\beta_m]$ [28, 60], where $\Delta > 0$ (< 0) indicates dynamical stability (instability) [50, 51]. With these notions, we can define the key diagnostic of boundary mode separability, the *Liouvillian separation gap*:

$$\Delta_s \equiv \Delta_{\text{bulk}} - \Delta_{\text{boundary}}, \quad (3)$$

where $\Delta_{\text{bulk}} = 2 \min_{m \neq 0} \text{Re}[\beta_m]$ and $\Delta_{\text{boundary}} = 2\text{Re}[\beta_0]$. A positive separation gap $\Delta_s > 0$ indicates that the boundary mode β_0 dominates long-time dynamics, either as the slowest decaying ($\text{Re}[\beta_0] > 0$) or fastest growing ($\text{Re}[\beta_0] < 0$) eigenmode, whereas a negative gap $\Delta_s < 0$ prevents boundary mode separation from bulk modes.

To obtain an analytical expression for the separation gap, we now focus on a class of real-space damping matrices in one dimension (1D): $X = \text{const} \cdot \mathbb{1} + iH_{\text{NH}}$, where H_{NH} is a generic nonreciprocal multi-band NH Hamiltonian. The open- and periodic-boundary rapidity spectra are related by an imaginary momentum shift [5, 17, 61], reflecting the emergence of a generalized Brillouin zone (GBZ) and the bulk skin effect. This correspondence is crucial because it allows to analytically resolve the entire spectrum under the open boundary condition (OBC), thereby enabling a controlled diagnosis of boundary-mode separation characterized by a positive Liouvillian separation gap.

Assume H_{NH} hosts a zero-energy boundary mode localized on sublattice A and vanishing on other sublattices denoted as \bar{A} . To dynamically isolate this mode, we consider two schemes: sublattice loss on \bar{A} (e.g. $L_{0,j}^l = \sqrt{\gamma_0^l} b_j$ for $j \in \bar{A}$) or sublattice gain on A (e.g. $L_{0,j}^g = \sqrt{\gamma_0^g} b_j^\dagger$ for $j \in A$), corresponding to distillation and amplification, respectively [Fig. 1(a) and (b)]. In both cases, sublattice dissipation enters X as a diagonal term $2\eta_0$ with $\eta_0 = \frac{1}{4}|\gamma_0^l| > 0$ (distillation) or $\eta_0 = -\frac{1}{4}|\gamma_0^g| < 0$ (amplification) [58]. For example, on a bipartite lattice indexed by the j -th unit cell $\underline{b}_j = (b_{j,A}, b_{j,\bar{A}})^T$, sublattice dissipation contributes to

$$\Delta X = \begin{cases} 2\eta_0 \times \text{diag}\{0, 1, 0, 1, \dots\}, & \eta_0 > 0 \\ 2\eta_0 \times \text{diag}\{1, 0, 1, 0, \dots\}, & \eta_0 < 0. \end{cases} \quad (4)$$

Acting as a uniform potential, η_0 plays two roles: it protects the boundary mode as an eigenmode of the new damping matrix $X \rightarrow X + \Delta X$, while keeping the GBZ description intact.

To illustrate our protocol, we consider a chiral two-band model represented in the GBZ with $H_{\text{NH}}^{\text{OBC}}(k) =$

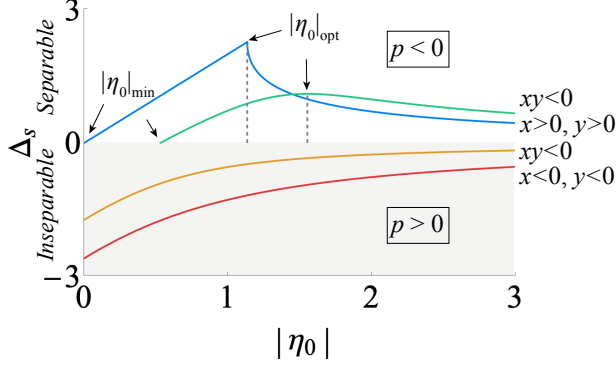


FIG. 2. **Liouvillian separation gap.** As a function of sub-lattice dissipation $|\eta_0|$, Δ_s is evaluated from analytically resolved expression in the large N limit for an odd-length chain [58]. We introduce auxiliary variables $\vec{z} = (t_1, t_2, \eta_1, \eta_2)$, $p = \eta_1^2 + \eta_2^2 - t_1^2 - t_2^2$, $x = |t_1| - |\eta_1|$, $y = |t_2| - |\eta_2|$. We choose representative parameters for four curves: (blue) $\vec{z} = (1, 2, 0.5, 0)$; (green) $\vec{z} = (0, 1.5, 0.5, 0.2)$; (yellow) $\vec{z} = (0.5, 0.5, 1, 0)$; (red) $\vec{z} = (0.25, 0.5, 0.5, 1)$.

$h_x(k)\sigma_x + h_y(k)\sigma_y$, and find

$$X(k) = (\eta_0 + \text{const}) \cdot \mathbb{1} + i\vec{h} \cdot \vec{\sigma}, \quad h_z = i\eta_0 \text{sgn}(\eta_0),$$

$$\Delta_s = \min_{\pm, k} 2\text{Re} \left[|\eta_0| \pm i\sqrt{h_x^2(k) + h_y^2(k) - \eta_0^2} \right]. \quad (5)$$

At $\eta_0 = 0$, $\Delta_s \leq 0$ due to spectral overlap. In the limit $|\eta_0| \rightarrow \infty$, the separation gap remains closed. Crucially, for intermediate sub-lattice dissipation $0 < |\eta_0| \ll \infty$, a positive Δ_s can emerge, dynamically isolating the boundary mode as the slowest decaying or fastest growing mode (Fig. 1 and Fig. 2). From Eq. (5), it follows that separability is generically possible when the nonreciprocity is not dominant, although it accommodates a large parameter space exhibiting a Liouvillian skin effect.

As a case study, next we focus on an exactly solvable NH Su-Schrieffer-Heeger (SSH) chain with an odd number of sites [29, 62], described by $H_{\text{NH}} = \sum_{j=1}^{N-1} (t_1^+ b_{j,A}^\dagger b_{j,B} + t_1^- b_{j,B}^\dagger b_{j,A} + t_2^+ b_{j,B}^\dagger b_{j+1,A} + t_2^- b_{j+1,A}^\dagger b_{j,B})$. The asymmetric hopping parameters $t_i^\pm = t_i \pm \eta_i \in \mathbb{R}$ enforce parity-time symmetry. H_{NH} supports an exact zero-energy boundary mode localized on sub-lattice A [6, 29]:

$$|\psi_{R/L,0}\rangle = \mathcal{N}_{R/L} \sum_{j=1}^N r_{R/L}^j b_{j,A}^\dagger |0\rangle,$$

$$r_R = -\frac{t_1^-}{t_2^+}, \quad r_L^* = -\frac{t_1^+}{t_2^-}, \quad (6)$$

with normalization factors $\mathcal{N}_{R/L}$. Nonreciprocity in H_{NH} can be introduced by correlated bond dissipation via reservoir engineering [63–66]: $L_{1,j}^l = \sqrt{\gamma_1^l} (b_{j,A} - ib_{j,B})$, $L_{1,j}^g = \sqrt{\gamma_1^g} (b_{j,A}^\dagger + ib_{j,B}^\dagger)$, $L_{2,j}^l = \sqrt{\gamma_2^l} (b_{j,B} - ib_{j+1,A})$, $L_{2,j}^g = \sqrt{\gamma_2^g} (b_{j,B}^\dagger + ib_{j+1,A}^\dagger)$. To implement OBC, we re-

move the B site in the last unit cell, adjusting the dissipation accordingly: $L_{1,N}^l = \sqrt{\gamma_1^l} b_{N,A}$, $L_{1,N}^g = \sqrt{\gamma_1^g} b_{N,A}^\dagger$, $L_{2,N}^l = -i\sqrt{\gamma_2^l} b_{1,A}$, $L_{2,N}^g = i\sqrt{\gamma_2^g} b_{1,A}^\dagger$.

Our bond-dissipative SSH model leads to a damping matrix of the form $X = (\eta_1 + \eta_2) \cdot \mathbb{1} + iH_{\text{NH}}$, with dissipation asymmetries $\eta_i = \frac{1}{2}(|\gamma_i^l| - |\gamma_i^g|)$. Using the GBZ formalism, we identify the bulk localization parameter

$$r = \sqrt{\frac{r_R}{r_L^*}} = \sqrt{\frac{t_1^- t_2^-}{t_1^+ t_2^+}}, \quad (7)$$

which enters the momentum shift $k \rightarrow k - i \ln r$ and determines the non-Bloch bulk spectrum:

$$h_x(k) = t_1 + t_2 \cos k + i\eta_2 \sin k,$$

$$h_y(k) = i\eta_1 - i\eta_2 \cos k + t_2 \sin k. \quad (8)$$

With additional sub-lattice dissipation η_0 in Eq. (4), the OBC rapidity spectrum of $X \rightarrow X + \Delta X$ in odd-length chains is mirror-symmetric under $k \rightarrow -k$, and its correspondence with the PBC spectrum becomes exact at all system sizes: $\beta_\pm^{\text{OBC}}(k) = \beta_\pm^{\text{PBC}}(k - i \ln r)$. This enables us to derive a fully analytical criterion for the emergence of a positive separation gap $\Delta_s > 0$ [58]:

$$\eta_1^2 + \eta_2^2 < t_1^2 + t_2^2, \quad |\eta_0| > |\eta_0|_{\min}. \quad (9)$$

This illustrates the general result that separability is possible for moderate nonreciprocity. More precisely, we uncover two dynamical regimes (Fig. 2): (1) a separable region ($\Delta_s > 0$), where the boundary mode can be cleanly isolated and made dynamically dominant; and (2) an inseparable region ($\Delta_s < 0$), where bulk and boundary real rapidities remain intermixed due to strong nonreciprocity. Our criterion provides an experimentally relevant roadmap for boundary-mode engineering in bosonic open systems.

In Fig. 2, an ideal separable case is identified when both $|t_1| > |\eta_1|$ and $|t_2| > |\eta_2|$ (blue curve), such that any finite η_0 suffices to induce separation, and the maximal gap occurs at $|\eta_0|_{\text{opt}}$: $(\Delta_s)_{\max} = 2|\eta_0|_{\text{opt}} = 2|\sqrt{t_1^2 - \eta_1^2} - \sqrt{t_2^2 - \eta_2^2}|$. This includes previously proposed Hermitian boundary mode preparation scheme at $\eta_{1,2} = 0$ [37]. Slightly increasing nonreciprocity by allowing $|t_1| < |\eta_1|$ (or $|t_2| < |\eta_2|$, green curve), separability requires tuning η_0 above a finite threshold $|\eta_0|_{\min} = \sqrt{\frac{(\eta_1^2 - t_1^2)(t_2^2 - \eta_2^2)}{t_1^2 + t_2^2 - \eta_1^2 - \eta_2^2}}$, but still yields a positive optimal gap (η_{opt} is resolved in Ref. [58]). In contrast, in the strong nonreciprocal regime ($\eta_1^2 + \eta_2^2 > t_1^2 + t_2^2$, yellow and red curves), separation fails entirely: here, the real part of $h_x^2 + h_y^2$ in Eq. (5) becomes negative, and η_0 cannot flip the sign of Δ_s to positive. Approaching topological transitions $|t_1^2 - \eta_1^2| = |t_2^2 - \eta_2^2|$, the positive gaps on two separable branches both shrink to zero, which is indicated by $(\Delta_s)_{\max} = 0$ at $t_1^2 - \eta_1^2 = t_2^2 - \eta_2^2$ (blue curve collapses to a flat zero line) and $|\eta_0|_{\min} = \infty$ at $t_1^2 - \eta_1^2 = -(t_2^2 - \eta_2^2)$.

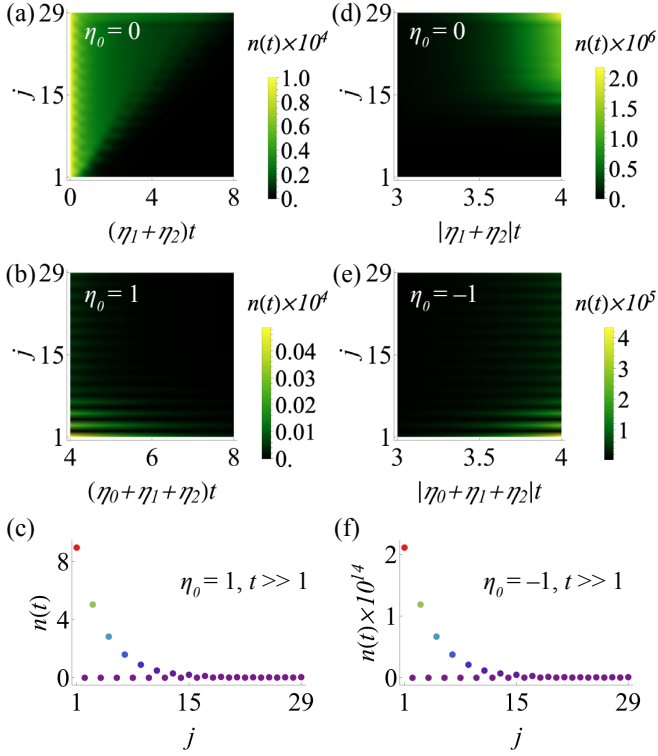


FIG. 3. **NH boundary mode dynamically selected by sublattice dissipation.** Distillation (a)–(c) and amplification (d)–(f) scenarios with $(t_1, t_2, \eta_1, \eta_2)$ set as in Fig. 1, and the initial configuration chosen at 10^4 bosons per site and vacuum, respectively. Boson density vs. time before/after adding sublattice dissipation is shown in (a),(d) and (b),(e), highlighting different localization tendencies of bulk and boundary modes: $r_{\xi, \text{bulk}} \simeq 1.73 > 1$ and $r_{\xi, \text{boundary}} = 0.75 < 1$. Sites with odd (even) index belong to sublattice A (B). With $|\eta_0| = 1$ close to $|\eta_0|_{\text{opt}} = 1.134$, the density in (c),(f) is dominated by the NH boundary mode at long times $|\eta_0 + \eta_1 + \eta_2|t = 10$.

(green curve becomes flat). It correctly signals a degeneracy between bulk and boundary rapidities.

We now present observable signatures of the boundary mode in separable regimes for the NH SSH model. A key observable which reflects both bulk and boundary skin effects is the boson density $n_j(t) = C_{jj}(t) = [\tilde{C}(t) + C_s]_{jj}$. It is possible to choose the parameter set $\{\eta_{i=0,1,2}\}$ to make the steady-state background uniform: $C_s \propto \mathbb{1}$, so that singularities are avoided (for instance, C_s has no solution when bond loss and gain are in global balance: $\eta_1 + \eta_2 = 0, \eta_0 = 0$ [58]). In the distillation (amplification) scheme where only loss (gain) is present: $\forall \eta_i \geq 0, C_s = 0$ ($\forall \eta_i \leq 0, C_s = -\mathbb{1}$). The Liouvillian gap Δ (the effective damping rate) shares the same sign as η_i , thereby ensuring that the distillation setup leads to a stable steady state (an empty chain), while the amplification setup results in diverging boson densities due to instability (Fig. 3).

Starting from the initial condition $C(0) = x \times \mathbb{1}$ (x

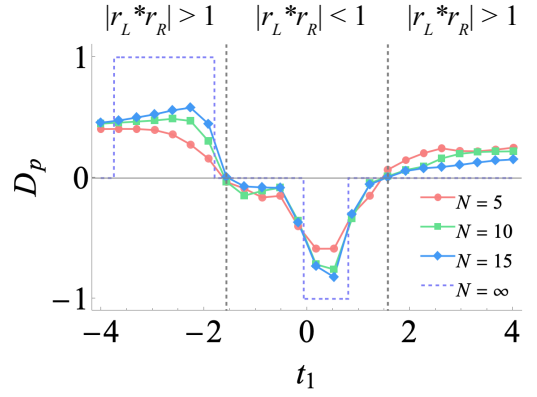


FIG. 4. **Polarization drift D_p alters sign across topological phase transitions.** We choose odd sites $n_{\text{tot}} = 2N - 1$ with N the number of unit cells and fix $t_2 = 1.5, \eta_1 = 0.5, \eta_2 = 0.2, \eta_0 = 1$. The dynamical polarization is measured at $t_{\text{max}} = 40$. Phase transitions (vertical dashed lines) occur at $|r_L^* r_R| = 1$ or $t_{1,c} = \pm \sqrt{t_2^2 - \eta_2^2 + \eta_1^2} \simeq \pm 1.568$, and are pinpointed by $D_p = 0$ given a finite system size N . In the thermodynamic limit, D_p converges to the bound (dashed in purple) predicted by Eq. (13).

bosons per site, $x \geq 0$), we can then analytically solve $n(t)$ using the diagonalized damping matrix [58]. From Eq. (2), it follows that the chiral damping of $n(t)$ is determined by localized left eigenvectors. Taking into account that sublattice dissipation in Eq. (4) protects localization lengths of both boundary and bulk modes [Eq. (6) and Eq. (7)], a successful boundary mode separation manifests at long times ($t \gg 1$) as

$$n_{j,A}(t) \propto |r_L|^{2j} e^{-\Delta_{\text{boundary}} t}, \quad n_{j,B}(t) \simeq 0, \quad (10)$$

where $\Delta_{\text{boundary}} = 2(\eta_1 + \eta_2 + \eta_0) - 2\eta_0 \text{sgn}(\eta_0)$. Otherwise, the dynamics are governed by bulk modes with

$$n_{j,A/B}(t) \propto |r|^{-2j} e^{-\Delta_{\text{bulk}} t}. \quad (11)$$

Fig. 3 shows the evolution of the boson density before and after switching on η_0 . At large times, panels (c) and (f) clearly reveal the boundary mode structure predicted by Eq. (10). Notably, the amplification scenario in panel (f) yields a highly populated and sharply localized boundary mode – suggesting potential application in NHSE-enhanced single-mode lasers [20].

Importantly, our separation scheme makes it possible to observe the NH BBC in open quantum systems. The chiral-symmetric non-Hermitian SSH chain is characterized by unconventional topological invariants: the non-Bloch winding number ν [5] or the biorthogonal polarization \mathcal{P} [6]. In the topological region $|r_L^* r_R| < 1$, $|\nu| = \mathcal{P} = 1$. At phase transitions $|r_L^* r_R| = 1$, due to the spectral crossing, the boundary mode enters the bulk and shares the same localization length: $r_{\xi, \text{boundary}} = r_{\xi, \text{bulk}}$ or $|r_L| = |r|^{-1}$ through Eq. (7). In our protocol, this critical phenomenon can be tracked down by measuring the long-time polarization [29, 36] with and without

boundary-mode separation. To elucidate, we define the *polarization drift* as

$$D_p(\eta_0) = P(\eta_0) - P(0), \quad |\eta_0| > |\eta_0|_{\min},$$

$$P(\eta_0) = \frac{\sum_{j=1}^{n_{\text{tot}}} j \cdot n_j(\eta_0, t)}{n_{\text{tot}} \cdot \sum_{j=1}^{n_{\text{tot}}} n_j(\eta_0, t)} \bigg|_{t=t_{\max} \gg 1}, \quad (12)$$

with $n_{\text{tot}} = 2N - 1$. Due to Liouvillian skin effects in Eqs. (10) and (11), $P(\eta_0)$ and $P(0)$ are governed by $r_{\xi, \text{boundary}} = |r_L|$ and $r_{\xi, \text{bulk}} = |r|^{-1}$ [Fig. 1 (c)]. Fig. 4 depicts the behavior of D_p with system size and highlights that $D_p \equiv 0$ at phase transitions. A trivial quantized bound appears in the thermodynamic limit (purple dashed curve):

$$D_p \xrightarrow{N \rightarrow \infty} \frac{1}{2} [\text{sgn}(\log |r_L|) - \text{sgn}(\log |r|^{-1})], \quad (13)$$

from the relation $\lim_{N \rightarrow \infty} P \simeq 1(0)$ if $r_\xi > 1(< 1)$. D_p becomes ± 1 when bulk and boundary modes are localized towards the same direction and fails to pinpoint critical lines (gray dashed). Remarkably, for small system size ($N = 10, 15$), D_p deviates from this bound and exhibits topological signatures – it drops to zero precisely at phase transitions and alters sign across them. Interestingly, D_p also responds to two of the exceptional points (EPs) of H_{NH} : $t_1^+ = 0$ and $t_2^- = 0$, where $|r_L| = |r|^{-1} = 0$ or ∞ . In Fig. 4, such an EP occurs at $t_1 = -\eta_1 = -0.5$. Yet, it has an order proportional to the system size and becomes unstable to any perturbation. As a result, while $D_p \simeq 0$ near these phenomenal EPs, it retains a consistent sign, further distinguishing true topological transitions from EP crossings. The sign switch of D_p thus provides a sharp and robust dynamical signature of NH topological phase transitions, enabled by boundary-mode separation.

By demonstrating how NH boundary modes can be generated, elevated, and utilized to dynamically characterize NH topology within a full open quantum setting, our work invites several theoretical generalizations. Once the solvability is broken, the boundary mode remains robust against bond disorder [37], persisting even in non-solvable chains with even lengths [58]. Our framework can also be extended to higher-dimensional and multi-band NH systems, including those without chiral symmetry [67, 68]. Another avenue is the refinement of dissipation schemes: generalizing sublattice loss to single-site dissipation [37] remains compatible with weak symmetries in the late-time mixed state [69, 70], potentially broadening applicability to single-band and interacting many-body systems [34, 71].

Acknowledgements. – We thank Christopher Ekman and Hui Liu for discussions. This work was supported by the Knut and Alice Wallenberg Foundation (KAW) via the Wallenberg Academy Scholars program (2023.0256) and the project Dynamic Quantum

Matter (2019.0068), the Swedish Research Council under the VR Starting Grant 2024-05213, and the Göran Gustafsson Foundation for Research in Natural Sciences and Medicine.

-
- [1] Y. Ashida, Z. Gong, and M. Ueda, Non-Hermitian physics, *Adv. Phys.* **69**, 249 (2020).
 - [2] E. J. Bergholtz, J. C. Budich, and F. K. Kunst, Exceptional topology of non-Hermitian systems, *Rev. Mod. Phys.* **93**, 015005 (2021).
 - [3] T. E. Lee, Anomalous edge state in a non-Hermitian lattice, *Phys. Rev. Lett.* **116**, 133903 (2016).
 - [4] Y. Xiong, Why does bulk boundary correspondence fail in some non-Hermitian topological models, *J. Phys. Commun.* **2**, 035043 (2018).
 - [5] S. Yao and Z. Wang, Edge states and topological invariants of non-Hermitian systems, *Phys. Rev. Lett.* **121**, 086803 (2018).
 - [6] F. K. Kunst, E. Edvardsson, J. C. Budich, and E. J. Bergholtz, Biorthogonal bulk-boundary correspondence in non-Hermitian systems, *Phys. Rev. Lett.* **121**, 026808 (2018).
 - [7] V. M. Martinez Alvarez, J. E. Barrios Vargas, and L. E. F. Foa Torres, Non-Hermitian robust edge states in one dimension: Anomalous localization and eigenspace condensation at exceptional points, *Phys. Rev. B* **97**, 121401 (2018).
 - [8] T. Helbig, T. Hofmann, S. Imhof, M. Abdelghany, T. Kiessling, L. Molenkamp, C. Lee, A. Szameit, M. Greiter, and R. Thomale, Generalized bulk–boundary correspondence in non-Hermitian topoelectrical circuits, *Nat. Phys.* **16**, 747–750 (2020).
 - [9] A. Ghatak, M. Brandenbourger, J. van Wezel, and C. Coulais, Observation of non-Hermitian topology and its bulk–edge correspondence in an active mechanical metamaterial, *PNAS* **117**, 29561 (2020).
 - [10] L. Xiao, T. Deng, K. Wang, G. Zhu, Z. Wang, W. Yi, and P. Xue, Non-Hermitian bulk–boundary correspondence in quantum dynamics, *Nat. Phys.* **16**, 761 (2020).
 - [11] M. Brandenbourger, X. Locsin, E. Lerner, and C. Coulais, Non-reciprocal robotic metamaterials, *Nat. Commun.* **10**, 4608 (2019).
 - [12] T. Hofmann, T. Helbig, F. Schindler, N. Salgo, M. Brzezińska, M. Greiter, T. Kiessling, D. Wolf, A. Vollhardt, A. Kabaši, C. H. Lee, A. Bilušić, R. Thomale, and T. Neupert, Reciprocal skin effect and its realization in a topoelectrical circuit, *Phys. Rev. Research* **2**, 023265 (2020).
 - [13] W. Wang, X. Wang, and G. Ma, Non-Hermitian morphing of topological modes, *Nature* **608**, 50–55 (2022).
 - [14] Q. Liang, D. Xie, Z. Dong, H. Li, H. Li, B. Gadway, W. Yi, and B. Yan, Dynamic signatures of non-Hermitian skin effect and topology in ultracold atoms, *Phys. Rev. Lett.* **129**, 070401 (2022).
 - [15] J. Veenstra, O. Gamayun, X.-F. Guo, A. Sarvi, C. V. Meinersen, and C. Coulais, Non-reciprocal topological solitons in active metamaterials, *Nature* **627**, 528–533 (2023).
 - [16] S. Yao, F. Song, and Z. Wang, Non-Hermitian Chern bands, *Phys. Rev. Lett.* **121**, 136802 (2018).

- [17] K. Yokomizo and S. Murakami, Non-Bloch band theory of non-Hermitian systems, *Phys. Rev. Lett.* **123**, 066404 (2019).
- [18] S. Ryu, A. P. Schnyder, A. Furusaki, and A. W. W. Ludwig, Topological insulators and superconductors: tenfold way and dimensional hierarchy, *New Journal of Physics* **12**, 065010 (2010).
- [19] M. Z. Hasan and C. L. Kane, Colloquium: Topological insulators, *Rev. Mod. Phys.* **82**, 3045 (2010).
- [20] B. Zhu, Q. Wang, D. Leykam, H. Xue, Q. J. Wang, and Y. Chong, Anomalous single-mode lasing induced by non-linearity and the non-Hermitian skin effect, *Phys. Rev. Lett.* **129**, 013903 (2022).
- [21] S. Weidemann, M. Kremer, T. Helbig, T. Hofmann, A. Stegmaier, M. Greiter, R. Thomale, and A. Szameit, Topological funneling of light, *Science* **368**, 311 (2020).
- [22] L. Li, C. H. Lee, and J. Gong, Topological switch for non-Hermitian skin effect in cold-atom systems with loss, *Phys. Rev. Lett.* **124**, 250402 (2020).
- [23] J. C. Budich and E. J. Bergholtz, Non-Hermitian topological sensors, *Phys. Rev. Lett.* **125**, 180403 (2020).
- [24] A. McDonald and A. A. Clerk, Exponentially-enhanced quantum sensing with non-Hermitian lattice dynamics, *Nat. Commun.* **11**, 5382 (2020).
- [25] F. Koch and J. C. Budich, Quantum non-Hermitian topological sensors, *Phys. Rev. Research* **4**, 013113 (2022).
- [26] O. Arandes and E. J. Bergholtz, Quantum sensing with driven-dissipative Su-Schrieffer-Heeger lattices, *arXiv:2412.13249*.
- [27] F. Song, S. Yao, and Z. Wang, Non-Hermitian skin effect and chiral damping in open quantum systems, *Phys. Rev. Lett.* **123**, 170401 (2019).
- [28] T. Haga, M. Nakagawa, R. Hamazaki, and M. Ueda, Liouvillian skin effect: Slowing down of relaxation processes without gap closing, *Phys. Rev. Lett.* **127**, 070402 (2021).
- [29] F. Yang, Q.-D. Jiang, and E. J. Bergholtz, Liouvillian skin effect in an exactly solvable model, *Phys. Rev. Research* **4**, 023160 (2022).
- [30] K. Kawabata, T. Numasawa, and S. Ryu, Entanglement phase transition induced by the non-Hermitian skin effect, *Phys. Rev. X* **13**, 021007 (2023).
- [31] S. Hamanaka, K. Yamamoto, and T. Yoshida, Interaction-induced Liouvillian skin effect in a fermionic chain with a two-body loss, *Phys. Rev. B* **108**, 155114 (2023).
- [32] C. Ekman and E. J. Bergholtz, Liouvillian skin effects and fragmented condensates in an integrable dissipative bose-hubbard model, *Phys. Rev. Res.* **6**, L032067 (2024).
- [33] Y.-M. Hu, Z. Wang, B. Lian, and Z. Wang, Many-body non-Hermitian skin effect with exact steady states in dissipative lattice gauge theory, *arXiv:2502.03534*.
- [34] R. D. Soares, M. Brunelli, and M. Schirò, Dissipative phase transition of interacting non-reciprocal fermions, *arXiv:2505.15711*.
- [35] Y. Shigedomi and T. Yoshida, Liouvillian skin effects in two-dimensional electron systems at finite temperatures, *2505.18001*.
- [36] R. Sarkar, S. S. Hegde, A. Narayan, and T. Meng, Chiral damping with persistent edge states: interplay of spectral topology and band topology in open quantum systems, *arXiv:2503.07193*.
- [37] F. Yang, P. Mognini, and E. J. Bergholtz, Dissipative boundary state preparation, *Phys. Rev. Research* **5**, 043229 (2023).
- [38] S. S. Hegde, T. Ehmcke, and T. Meng, Edge-selective extremal damping from topological heritage of dissipative Chern insulators, *Phys. Rev. Lett.* **131**, 256601 (2023).
- [39] F. Yang, Z. Wei, X. Tong, K. Cao, and S.-P. Kou, Symmetry classes of dissipative topological insulators with edge dark states, *Phys. Rev. B* **107**, 165139 (2023).
- [40] Y. Peng, C. Yang, H. Hu, and Y. Wang, Dissipation-assisted preparation of topological boundary states, *arXiv:2412.04152*.
- [41] E.-S. Ma, K.-L. Zhang, and Z. Song, Dynamically stable topological edge states in an extended Su-Schrieffer-Heeger ladder with balanced perturbation, *arXiv:2506.05666*.
- [42] T. Prosen, Third quantization: A general method to solve master equations for quadratic open Fermi systems, *New J. Phys.* **10**, 043026 (2008).
- [43] T. Prosen and B. Žunkovič, Exact solution of Markovian master equations for quadratic Fermi systems: Thermal baths, open XY spin chains and non-equilibrium phase transition, *New J. Phys.* **12**, 025016 (2010).
- [44] T. Prosen, Spectral theorem for the Lindblad equation for quadratic open fermionic systems, *J. Stat. Mech.* **2010**, P07020 (2010).
- [45] J. Eisert and T. Prosen, Noise-driven quantum criticality, *arXiv:1012.5013*.
- [46] V. Alba and F. Carollo, Spreading of correlations in Markovian open quantum systems, *Phys. Rev. B* **103**, L020302 (2021).
- [47] A. McDonald and A. A. Clerk, Third quantization of open quantum systems: Dissipative symmetries and connections to phase-space and Keldysh field-theory formulations, *Phys. Rev. Research* **5**, 033107 (2023).
- [48] A. McDonald, R. Hanai, and A. A. Clerk, Non-equilibrium stationary states of quantum non-Hermitian lattice models, *Phys. Rev. B* **105**, 064302 (2022).
- [49] Y.-M. Hu, W.-T. Xue, F. Song, and Z. Wang, Steady-state edge burst: From free-particle systems to interaction-induced phenomena, *Phys. Rev. B* **108**, 235422 (2023).
- [50] T. Prosen and T. H. Seligman, Quantization over boson operator spaces, *J. Phys. A Math. Theor.* **43**, 392004 (2010).
- [51] M. Ughrelidze, V. P. Flynn, E. Cobanera, and L. Viola, Interplay of finite-and infinite-size stability in quadratic bosonic Lindbladians, *Phys. Rev. A* **110**, 032207 (2024).
- [52] C. C. Wanjura, M. Brunelli, and A. Nunnenkamp, Topological framework for directional amplification in driven-dissipative cavity arrays, *Nature Communications* **11**, 3149 (2020).
- [53] L. Feng, Z. J. Wong, R.-M. Ma, Y. Wang, and X. Zhang, Single-mode laser by parity-time symmetry breaking, *Science* **346**, 972 (2014).
- [54] M. Parto, S. Wittek, H. Hodaei, G. Harari, M. A. Bandres, J. Ren, M. C. Rechtsman, M. Segev, D. N. Christodoulides, and M. Khajavikhan, Edge-mode lasing in 1D topological active arrays, *Phys. Rev. Lett.* **120**, 113901 (2018).
- [55] S. Lieu, M. McGinley, and N. R. Cooper, Tenfold way for quadratic Lindbladians, *Phys. Rev. Lett.* **124**, 040401 (2020).
- [56] G. Lindblad, On the generators of quantum dynamical semigroups, *Commun. Math. Phys.* **48**, 119 (1976).
- [57] H.-P. Breuer, F. Petruccione, *et al.*, *The theory of open*

- quantum systems* (Oxford University Press, 2007).
- [58] See Supplementary Material for details on two derivations of NH damping matrix using third quantization and the equation of motion of two-point correlator, together with exact solutions to an odd-length chain under OBC. Solvable lines and singularities for a unique bosonic reference steady state (BRSS) are presented as well. Dynamical observables are obtained based on the BRSS. We also analytically resolve the Liouvillian separation gap in the large N limit and calculate numerically the signals in the polarization drift for a non-solvable even-length chain.
 - [59] D. C. Brody, Biorthogonal quantum mechanics, *J. Phys. A* **47**, 035305 (2013).
 - [60] F. Minganti, A. Biella, N. Bartolo, and C. Ciuti, Spectral theory of Liouvillians for dissipative phase transitions, *Phys. Rev. A* **98**, 042118 (2018).
 - [61] F. K. Kunst and V. Dwivedi, Non-Hermitian systems and topology: A transfer-matrix perspective, *Phys. Rev. B* **99**, 245116 (2019).
 - [62] E. Edvardsson, F. K. Kunst, T. Yoshida, and E. J. Bergholtz, Phase transitions and generalized biorthogonal polarization in non-Hermitian systems, *Phys. Rev. Research* **2**, 043046 (2020).
 - [63] A. Metelmann and A. A. Clerk, Nonreciprocal photon transmission and amplification via reservoir engineering, *Phys. Rev. X* **5**, 021025 (2015).
 - [64] A. Clerk, Introduction to quantum non-reciprocal interactions: from non-Hermitian Hamiltonians to quantum master equations and quantum feedforward schemes, *SciPost Phys. Lect. Notes.*, 044 (2022).
 - [65] P. He, Y.-G. Liu, J.-T. Wang, and S.-L. Zhu, Damping transition in an open generalized Aubry-André-Harper model, *Phys. Rev. A* **105**, 023311 (2022).
 - [66] S. E. Begg and R. Hanai, Quantum criticality in open quantum spin chains with nonreciprocity, *Phys. Rev. Lett.* **132**, 120401 (2024).
 - [67] H.-Y. Wang, F. Song, and Z. Wang, Amoeba formulation of non-Bloch band theory in arbitrary dimensions, *Phys. Rev. X* **14**, 021011 (2024).
 - [68] F. Yang and E. J. Bergholtz, Anatomy of higher-order non-Hermitian skin and boundary modes, *Phys. Rev. Research* **7**, 023233 (2025).
 - [69] B. Buča and T. Prosen, A note on symmetry reductions of the Lindblad equation: transport in constrained open spin chains, *New J. Phys.* **14**, 073007 (2012).
 - [70] Z.-M. Huang, S. Diehl, and X.-Q. Sun, Topological response in open quantum systems with weak symmetries, [arXiv:2504.02941](#).
 - [71] H.-R. Wang, Z. Wang, and Z. Wang, Non-Bloch self-energy of dissipative interacting fermions, [arXiv:2411.13661](#).

Supplementary Material for “Quantum dynamical signatures of non-Hermitian boundary modes”

In the supplementary material, we study the dynamics of a bosonic SSH chain with coherent bond and sublattice dissipation in more detail. First, we provide the derivation of non-Hermitian (NH) damping matrix using third quantization and the equation of motion of two-point correlation function. Exact solutions to the damping matrix are found for odd sites under open boundary conditions (OBC). Second, we discuss the existence of solutions to the Lyapunov equation with globally balanced bond loss and gain as singularities. Solvable lines are identified for a unique bosonic reference steady state (BRSS). Along these lines, we analyze dynamical observables, the stability of the BRSS as well as phenomena close to singularities. Moreover, we resolve analytically Liouvillian separation gap between NH bulk and boundary modes. Lastly, as a comparison the polarization drift is numerically calculated for a non-solvable even-length chain.

Non-Hermitian damping matrix

To begin with, we present two equivalent methods to derive NH damping matrix of the dissipative bosonic SSH chain. In the first approach, we apply third quantization over unbounded Liouville space of bosons and diagonalize the quadratic Lindbladian. In the second one, following commutation relations of bosonic operators, we resolve the time evolution of two-point correlation function. In the end, we construct exact solutions to NH damping matrix for an odd-length chain under OBC.

Third quantization of quadratic bosonic Lindbladians

Third quantization has been generalized to solve Lindblad master equation in open bosonic systems [50] with recently proposed reformulations and connections to Keldysh field-theory approach [47]. In the following, we give a brief review of the original formalism [50] and make links with open Fermi matter [29, 42–44].

Let us denote the unbounded Liouville space of bosons as \mathcal{K} . To find its Fock basis, given density operator $\rho \in \mathcal{K}$, we introduce left and right multiplication maps for each bosonic operator on the j -th site: $b_j^L \rho = b_j \rho$, $b_j^{\dagger L} \rho = b_j^\dagger \rho$ and $b_j^R \rho = \rho b_j$, $b_j^{\dagger R} \rho = \rho b_j^\dagger$. A new set of operators can be built

$$b_{0,j} = b_j^L, \quad b'_{0,j} = b_j^{\dagger L} - b_j^{\dagger R}, \quad b_{1,j} = b_j^{\dagger R}, \quad b'_{1,j} = b_j^R - b_j^L, \quad (14)$$

such that they satisfy commutation relations of bosons over space \mathcal{K} :

$$[b_{\nu,j}, b'_{\mu,k}] = \delta_{\nu,\mu} \delta_{j,k}, \quad [b_{\nu,j}, b_{\mu,k}] = [b'_{\nu,j}, b'_{\mu,k}] = 0, \quad \nu, \mu \in \{0, 1\}. \quad (15)$$

While the vacuum of \mathcal{K} is a pure state $\rho_0 = |\psi_0\rangle\langle\psi_0|$ determined by annihilation operators b_ν , the Fock basis $|\underline{\alpha}\rangle$ is unbounded built on creation operators b'_ν :

$$b_{\nu,j} \rho_0 = 0, \quad \forall \nu, \forall j; \\ |\underline{\alpha}\rangle = \prod_{\nu,j} \frac{(b'_{\nu,j})^{\alpha_{\nu,j}}}{\sqrt{\alpha_{\nu,j}!}} \rho_0, \quad \alpha_{\nu,j} \in \mathbb{Z}_+. \quad (16)$$

We adopt the notation $\underline{x} = (x_1, x_2, \dots, x_n)^T$ to represent a column vector of scalars or operators. And $\underline{\alpha} = (\alpha_{0,1}, \alpha_{1,1}, \alpha_{0,2}, \alpha_{1,2}, \dots, \alpha_{0,n}, \alpha_{1,n})^T$ consists of $2n$ components for a system of n sites. In open Fermi matter, the Liouville space is expanded by a basis of Majorana fermions, the occupation number of which is restricted by Pauli exclusion principle $\alpha_j \in \{0, 1\}$. Here, the Boson number, in contrast, is unbounded $\alpha_{\nu,j} \in \{0, 1, 2, 3, \dots\}$.

Applying left and right multiplication maps, the bosonic Liouvillian shares the form over space \mathcal{K} :

$$\hat{\mathcal{L}} = -i(\mathcal{H}^L - \mathcal{H}^R) + \sum_{\mu} [L_{\mu}^L L_{\mu}^{\dagger R} - \frac{1}{2}(L_{\mu}^{\dagger L} L_{\mu}^L + L_{\mu}^R L_{\mu}^{\dagger R})], \quad (17)$$

where under the notation $\underline{b} = (b_1, b_2, \dots, b_n)^T$, we denote

$$\mathcal{H} = \underline{b}^\dagger \cdot H \underline{b}, \quad L_{\mu}^l = \underline{l}_{\mu} \cdot \underline{b}, \quad L_{\mu}^g = \underline{g}_{\mu} \cdot \underline{b}^\dagger. \quad (18)$$

In our model, the general Lindblad operators L^l (L^g) describe coherent loss (gain) on bonds and on two sublattices with the subscript μ differentiating each type.

Changing to the basis $\underline{d} = (\underline{a}, \underline{a}')^T = (\underline{b}_0, \underline{b}_1, \underline{b}'_0, \underline{b}'_1)^T$ through the mapping in Eq. (14), one arrives at a quadratic Liouvillian

$$\hat{\mathcal{L}} = \underline{d}^T \cdot S \underline{d} - S_0 \cdot \mathbb{1}_{4n \times 4n}. \quad (19)$$

The $4n \times 4n$ matrix S takes the form

$$S = \begin{pmatrix} 0 & -\tilde{X} \\ -\tilde{X}^T & Y \end{pmatrix}, \quad \tilde{X} = \frac{1}{2} \begin{pmatrix} X & 0 \\ 0 & X^* \end{pmatrix}, \quad Y = \frac{1}{2} \begin{pmatrix} 0 & (M^g)^T \\ M^g & 0 \end{pmatrix}, \quad (20)$$

with elements consisting of $n \times n$ matrices

$$X = iH^T + \frac{1}{2}[(M^l)^T - M^g], \quad \mathcal{H} = \sum_{jk} b_j^\dagger H_{jk} b_k, \quad M^l = \sum_{\mu} l_{\mu}^\dagger l_{\mu}, \quad M^g = \sum_{\mu} g_{\mu}^\dagger g_{\mu}. \quad (21)$$

And the scalar reads $S_0 = \text{Tr} \tilde{X} = \frac{1}{2}[\text{Tr}(M^l) - \text{Tr}(M^g)]$. We thus obtain NH damping matrix X that governs relaxation dynamics of quadratic Lindbladians.

Next, we show the bosonic Liouvillian can be diagonalized by the same set of eigen solutions to the enlarged NH damping matrix \tilde{X} in Eq. (20), if there exists a unique solution to the continuous Lyapunov equation:

$$\tilde{X}^T Z + Z \tilde{X} = Y. \quad (22)$$

By analogy to fermions, the covariance matrix Z encodes the structure of a bosonic reference steady state (BRSS). It is useful to further simplify the Lyapunov equation into the form:

$$X^\dagger C_s + C_s X = M^g, \quad (23)$$

by introducing

$$Z = \begin{pmatrix} 0 & C_s^* \\ C_s^\dagger & 0 \end{pmatrix}. \quad (24)$$

Here, C_s gives the two-point correlation matrix of BRSS. The existence and uniqueness of the solution C_s will be discussed in more details in the next section.

Compared with Ref. [50], we now present a slightly different yet simple method to diagonalize the Liouvillian using transformation matrices. It can be checked that given covariance matrix Z satisfying Lyapunov equation in Eq. (22), the Liouvillian shares a block-diagonalized form:

$$S = J^{-1} W \begin{pmatrix} -\tilde{X}^T & 0 \\ 0 & \tilde{X} \end{pmatrix} W^{-1}, \quad (25)$$

where two transformation matrices read

$$J = \begin{pmatrix} 0 & 1 \\ -1 & 0 \end{pmatrix}, \quad W = \begin{pmatrix} 1 & Z \\ 0 & 1 \end{pmatrix}. \quad (26)$$

It leads to

$$\hat{\mathcal{L}} = (\underline{v}'^T \quad -\underline{v}^T) \cdot \begin{pmatrix} -\tilde{X}^T & 0 \\ 0 & \tilde{X} \end{pmatrix} \begin{pmatrix} \underline{v} \\ \underline{v}' \end{pmatrix} - \text{Tr} \tilde{X} \cdot \mathbb{1}, \quad (27)$$

with a change of basis

$$\begin{pmatrix} \underline{v} \\ \underline{v}' \end{pmatrix} = W^{-1} \underline{d} = \begin{pmatrix} \underline{a} - Z \underline{a}' \\ \underline{a}' \end{pmatrix}, \quad [v_j, v'_k] = \delta_{j,k}. \quad (28)$$

Since the enlarged NH damping matrix \tilde{X} in our model is diagonalizable via the non-unitary matrix U ,

$$\tilde{X} = U\Sigma U^{-1}, \quad \Sigma = \text{diag}\{\tilde{\beta}_1, \dots, \tilde{\beta}_{2n}\}, \quad (29)$$

one arrives at a Liouvillian decomposed in its normal master modes (NMMs):

$$\hat{\mathcal{L}} = -2 \sum_{m=1}^{2n} \tilde{\beta}_m \underline{\zeta}'_m \cdot \underline{\zeta}_m, \quad (30)$$

where m denotes the band index and NMMs are given by

$$\underline{\zeta} = U^T \underline{v}, \quad \underline{\zeta}' = U^{-1} \underline{v}'. \quad (31)$$

Taking into account Eq. (28), NMMs also satisfy bosonic commutation relations: $[\underline{\zeta}_m, \underline{\zeta}'_l] = \delta_{m,l}$.

So far, we prove that the rapidity spectrum $\tilde{\beta} = \{\tilde{\beta}_1, \dots, \tilde{\beta}_{2n}\}$ of $\hat{\mathcal{L}}$ shares same eigenvalues of \tilde{X} , the matrix structure of which in Eq. (20) is enlarged from NH damping matrix X . It results in a combination of complex conjugate pairs:

$$\tilde{\beta} = \left\{ \frac{1}{2}\beta, \frac{1}{2}\beta^* \right\}, \quad (32)$$

with β denoting n eigenvalues of X . Combined with extra factor 2 in Eq. (30), hereafter we refer to $\{\beta_m\}$ as rapidity spectrum.

In the end, going back to our model, we are interested in a bosonic SSH chain under OBC:

$$\mathcal{H} = \sum_{j=1}^{N-1} t_1 b_{j,A}^\dagger b_{j,B} + t_2 b_{j+1,A}^\dagger b_{j,B} + h.c., \quad (33)$$

with coherent loss and gain on t_1 and t_2 bonds:

$$\begin{aligned} j = 1, \dots, N-1 : \quad & \begin{cases} L_{1,j}^l = \sqrt{\gamma_1^l} (b_{j,A} - i b_{j,B}) \\ L_{1,j}^g = \sqrt{\gamma_1^g} (b_{j,A}^\dagger + i b_{j,B}^\dagger) \end{cases}, \quad \begin{cases} L_{2,j}^l = \sqrt{\gamma_2^l} (b_{j,B} - i b_{j+1,A}) \\ L_{2,j}^g = \sqrt{\gamma_2^g} (b_{j,B}^\dagger + i b_{j+1,A}^\dagger) \end{cases}, \\ j = N : \quad & \begin{cases} L_{1,N}^l = \sqrt{\gamma_1^l} b_{N,A} \\ L_{1,N}^g = \sqrt{\gamma_1^g} b_{N,A}^\dagger \end{cases}, \quad \begin{cases} L_{2,N}^l = (-i) \sqrt{\gamma_2^l} b_{1,A} \\ L_{2,N}^g = i \sqrt{\gamma_2^g} b_{1,A}^\dagger \end{cases}, \end{aligned} \quad (34)$$

and loss on sublattice B and gain on sublattice A :

$$\forall j : \quad L_{0,j}^l = \sqrt{\gamma_0^l} b_{j,B}, \quad L_{0,j}^g = \sqrt{\gamma_0^g} b_{j,A}. \quad (35)$$

Correspondingly, the $n \times n$ damping matrix with $n = n_{\text{tot}} = 2N - 1$ total number of sites, as well as loss and gain matrices $M^\nu (\nu = g, l)$ in Eq. (21) hold the structures under OBC:

$$X = (\eta_0 + \eta_1 + \eta_2) \cdot \mathbb{1}_{n \times n} + i H_{\text{NH}}, \quad H_{\text{NH}} = H_S + i \Upsilon, \quad (36)$$

with

$$\begin{aligned} H_S = & \begin{pmatrix} 0 & t_1^+ & & & \\ t_1^- & 0 & t_2^+ & & \\ & t_2^- & 0 & & \\ & & & \ddots & \\ & & & & 0 & t_1^+ \\ & & & & t_1^- & 0 & t_2^+ \\ & & & & & t_2^- & 0 \end{pmatrix}, \quad \Upsilon = \frac{i}{4} (|\gamma_0^l| + |\gamma_0^g|) \times \text{diag}\{1, -1, 1, -1, \dots, 1\}_{n \times n}, \\ M^\nu = & \left(\frac{1}{2} |\gamma_0^\nu| + |\gamma_1^\nu| + |\gamma_2^\nu| \right) \cdot \mathbb{1}_{n \times n} + i (-1)^\nu \begin{pmatrix} -\frac{i}{2} |\gamma_0^\nu| & |\gamma_1^\nu| & & & \\ -|\gamma_1^\nu| & \frac{i}{2} |\gamma_0^\nu| & |\gamma_2^\nu| & & \\ & -|\gamma_2^\nu| & -\frac{i}{2} |\gamma_0^\nu| & & \\ & & & \ddots & \\ & & & & -\frac{i}{2} |\gamma_0^\nu| & |\gamma_1^\nu| \\ & & & & -|\gamma_1^\nu| & \frac{i}{2} |\gamma_0^\nu| & |\gamma_2^\nu| \\ & & & & & -|\gamma_2^\nu| & -\frac{i}{2} |\gamma_0^\nu| \end{pmatrix}, \end{aligned} \quad (37)$$

where $(-1)^\nu = +1$ (-1) for $\nu = g$ (l), and the matrix elements read

$$i = 1, 2: \quad t_i^\pm = t_i \pm \eta_i, \quad \eta_i = \frac{1}{2}(|\gamma_i^l| - |\gamma_i^g|); \quad \eta_0 = \frac{1}{4}(|\gamma_0^l| - |\gamma_0^g|). \quad (38)$$

In Eq. (36), one maps the NH damping matrix X to the Hamiltonian of NH SSH chain H_S with additional sublattice potential Υ . Compared with fermions [29], the asymmetric hopping terms (η_1, η_2) in bosonic H_S are determined by the imbalance between bond loss and gain rather than their total strength.

Equation of motion of two-point correlation function

Next, we provide an alternative derivation for NH damping matrix in Eq. (21) through the equation of motion of single-particle correlation function. One can choose either a real symmetric basis composed of position and momentum operators for bosons [45]: $u_{1,j} = b_j + b_j^\dagger$ and $u_{2,j} = i(b_j - b_j^\dagger)$, or a complex boson basis [47]: b_j and b_j^\dagger . The two representations correspond to Majorana fermion basis [46] and complex fermion basis [27] in open fermionic systems. We will apply the complex boson basis to our model.

Let us define two-point correlation function: $C_{jk}(t) = \text{Tr}[\rho(t)b_j^\dagger b_k]$. From the Lindblad master equation in Eq. (1), its time evolution consists of three parts: $\partial_t C = A^0 + A^l + A^g$, with contributions coming from \mathcal{H} , L_μ^l and L_μ^g respectively. Combined with the cyclic property of the trace and commutation relations of bosons $[b_j, b_k^\dagger] = \delta_{j,k}$, one can resolve each part straightforwardly. By definitions in Eq. (18) and Eq. (21), we obtain

$$\begin{aligned} A_{jk}^0 &= -i \sum_{mn} H_{mn} \text{Tr}([b_m^\dagger b_n, \rho] b_j^\dagger b_k) \\ &= -i \sum_{mn} H_{mn} \text{Tr}(\rho [b_j^\dagger b_k, b_m^\dagger b_n]) \\ &= -i \sum_{mn} H_{mn} \text{Tr}(\rho (b_j^\dagger [b_k, b_m^\dagger] b_n - b_m^\dagger [b_n, b_j^\dagger] b_k)) \\ &= i \sum_m H_{jm}^T C_{mk} - i \sum_n C_{jn} H_{nk}^T, \\ A_{jk}^l &= \sum_{mn} M_{mn}^l \text{Tr}(b_n \rho b_m^\dagger b_j^\dagger b_k - \frac{1}{2} \{b_m^\dagger b_n, \rho\} b_j^\dagger b_k) \\ &= \sum_{mn} M_{mn}^l \text{Tr}(\rho (b_m^\dagger [b_j^\dagger b_k, b_n] + \frac{1}{2} [b_m^\dagger b_n, b_j^\dagger b_k])) \\ &= \sum_{mn} M_{mn}^l \text{Tr}(\rho (-\frac{1}{2} b_m^\dagger [b_n, b_j^\dagger] b_k - \frac{1}{2} b_j^\dagger [b_k, b_m^\dagger] b_n)) \\ &= -\frac{1}{2} \sum_m (M^l)_{jm}^T C_{mk} - \frac{1}{2} \sum_n C_{jn} (M^l)_{nk}^T, \\ A_{jk}^g &= \sum_{mn} M_{mn}^g \text{Tr}(b_n^\dagger \rho b_m b_j^\dagger b_k - \frac{1}{2} \{b_m b_n^\dagger, \rho\} b_j^\dagger b_k) \\ &= \sum_{mn} M_{mn}^g \text{Tr}(\rho (b_m [b_j^\dagger b_k, b_n^\dagger] - \frac{1}{2} [b_j^\dagger b_k, b_m b_n^\dagger])) \\ &= \sum_{mn} M_{mn}^g \text{Tr}(\rho (\frac{1}{2} b_j^\dagger b_m [b_k, b_n^\dagger] + \frac{1}{2} [b_m, b_j^\dagger] b_n^\dagger b_k + \delta_{m,j} [b_k, b_n^\dagger])) \\ &= \frac{1}{2} \sum_n M_{jn}^g C_{nk} + \frac{1}{2} \sum_m C_{jm} M_{mk}^g + M_{jk}^g. \end{aligned} \quad (39)$$

As a result, the equation of motion of two-point correlator follows the form:

$$\begin{aligned} \partial_t C(t) &= -X^\dagger C(t) - C(t)X + M^g, \\ X &= iH^T + \frac{1}{2}[(M^l)^T - M^g]. \end{aligned} \quad (40)$$

We have employed the Hermiticity of H , M^l and M^g in Eq. (21). The same structure of NH damping matrix is thus retrieved. By setting $\partial_t C_s = 0$ for BRSS, one recovers the simplified Lyapunov equation in Eq. (23).

Exact solutions to NH damping matrix on an odd-length chain

We are interested in three types of dissipative setups: loss and gain on bonds ($\eta_0 = 0$, $|\gamma_0^l| = |\gamma_0^g| = 0$), loss on bonds and B -sublattice ($\eta_0 = \frac{1}{4}|\gamma_0^l| > 0$, $|\gamma_i^g| = 0, \forall i$), gain on bonds and A -sublattice ($\eta_0 = -\frac{1}{4}|\gamma_0^g| < 0$, $|\gamma_i^l| = 0, \forall i$), which bring NH Hamiltonians in Eq. (37):

$$H_{\text{NH}} = \begin{pmatrix} 0 & t_1^+ & 0 \\ t_1^- & 0 & t_2^+ \\ 0 & t_2^- & 0 \\ & & & \ddots \end{pmatrix}, \quad \begin{pmatrix} i\eta_0 & t_1^+ & 0 \\ t_1^- & -i\eta_0 & t_2^+ \\ 0 & t_2^- & i\eta_0 \\ & & & \ddots \end{pmatrix}, \quad \begin{pmatrix} -i\eta_0 & t_1^+ & 0 \\ t_1^- & i\eta_0 & t_2^+ \\ 0 & t_2^- & -i\eta_0 \\ & & & \ddots \end{pmatrix}. \quad (41)$$

The damping matrix $X = (\eta_0 + \eta_1 + \eta_2) \cdot \mathbb{1} + iH_{\text{NH}}$ shares the same right and left eigenvectors with H_{NH} . From the eigenvalue equations,

$$H_{\text{NH}} \underline{\psi}_{Rm} = \epsilon_m \underline{\psi}_{Rm}, \quad H_{\text{NH}}^\dagger \underline{\psi}_{Lm} = \epsilon_m^* \underline{\psi}_{Lm}, \quad (42)$$

the rapidity spectrum of X renders

$$\beta_m = (\eta_0 + \eta_1 + \eta_2) + i\epsilon_m. \quad (43)$$

Once the eigenvectors satisfy biorthogonal relations [59]:

$$\underline{\psi}_{Lm}^* \cdot \underline{\psi}_{Rl} = \delta_{m,l}, \quad (44)$$

NH damping matrix can be decomposed into the form

$$X = \sum_m \beta_m |\underline{\psi}_{R,m}\rangle \langle \underline{\psi}_{L,m}|. \quad (45)$$

This decomposition applies to the diagonalization procedure of $\hat{\mathcal{L}}$ in Eq. (20) and Eq. (29).

With odd sites $n_{\text{tot}} = 2N - 1$ under OBC, the damping matrix is exactly solvable due to spectral mirror symmetry. First, H_{NH} from three settings of Eq. (41) share one boundary mode with a structure exponentially localized on the sublattice A and fully suppressed on the sublattice B [6]:

$$|\psi_{R/L,0}\rangle = \mathcal{N}_{R/L} \sum_{j=1}^N r_{R/L}^j b_{A,j}^\dagger |0\rangle. \quad (46)$$

The localization parameters are given by

$$r_R = -\frac{t_1^-}{t_2^+}, \quad r_L^* = -\frac{t_1^+}{t_2^-}. \quad (47)$$

Here, we introduce normalization factors $\mathcal{N}_{R/L}$ to meet the biorthogonal relation $\langle \psi_{L0} | \psi_{R0} \rangle = 1$, and

$$\mathcal{N}_L^* \mathcal{N}_R = \begin{cases} (r_L^* r_R - 1) \{ (r_L^* r_R) [(r_L^* r_R)^N - 1] \}^{-1}, & |r_L^* r_R| \neq 1; \\ N^{-1}, & r_L^* r_R = 1; \\ [(-1)^N - 1]/2, & r_L^* r_R = -1. \end{cases} \quad (48)$$

Yet, the eigenvalue of this boundary mode becomes different in three settings:

$$\epsilon_0 = 0, \quad i\eta_0, \quad -i\eta_0. \quad (49)$$

For bulk skin modes, their OBC spectrum can be obtained from the PBC one by an imaginary momentum shift [5, 61]:

$$\epsilon_\pm^{\text{OBC}}(k) = \epsilon_\pm^{\text{PBC}}(k - i \ln r), \quad (50)$$

with band index $m = \{\pm, k\}$ and discrete momentum $k = \pi \cdot m/N, m = 1, 2, \dots, N-1$. The bulk energies come in pairs: $\epsilon_+ = -\epsilon_-$. Spectral mirror symmetry $\epsilon_\pm^{\text{OBC}}(k) = \epsilon_\pm^{\text{OBC}}(-k)$ [29, 62] ensures that the relation of Eq. (50) leads

to an exact OBC bulk spectrum. From non-unitary gauge transforms [5, 29], we determine the imaginary momentum shift for H_{NH} as

$$r = \sqrt{\frac{t_1^- t_2^-}{t_1^+ t_2^+}}. \quad (51)$$

It defines the generalized Brillouin zone (GBZ) [5, 17], of which the non-Bloch phase factor has a modulus different from 1: $e^{ikx} \rightarrow r e^{ikx}$, $|r| \neq 1$. r also characterizes the exponential localization behaviour of bulk skin modes. The non-Bloch Hamiltonian in the GBZ takes the form

$$H_{\text{NH}}^{\text{non-Bloch}}(k) = H_{\text{NH}}^{\text{Bloch}}(k - i \ln r) = \vec{h} \cdot \vec{\sigma} = \begin{pmatrix} h_z & h_x - i h_y \\ h_x + i h_y & -h_z \end{pmatrix}, \quad (52)$$

where

$$h_x = t_1 + t_2 \cos(k) + i \eta_2 \sin(k), \quad h_y = i \eta_1 - i \eta_2 \cos(k) + t_2 \sin(k), \quad (53)$$

and the σ^z component corresponding to three setups in Eq. (41) follows

$$h_z = 0, \quad i \eta_0, \quad -i \eta_0. \quad (54)$$

The eigenenergies become

$$\epsilon_{\pm}(k) = \pm \sqrt{h_x^2 + h_y^2 + h_z^2} = \pm h, \quad (55)$$

with

$$\epsilon_{\pm}(k) = \pm \sqrt{t_1^2 + t_2^2 - \eta_1^2 - \eta_2^2 + \text{sgn}[(t_1 + \eta_1)(t_2 + \eta_2)] \cdot 2 \sqrt{(t_1^2 - \eta_1^2)(t_2^2 - \eta_2^2) \cos(k) - \eta_0^2}}. \quad (56)$$

A sgn function is added to produce the correct sign for our convention of r in Eq. (51). The associated eigenvectors of the non-Bloch Hamiltonian

$$\underline{u}_{R,\pm}^{\text{OBC}}(k) = \frac{1}{\sqrt{2h(h \mp h_z)}} \begin{pmatrix} h_x - i h_y \\ \pm h - h_z \end{pmatrix}, \quad \underline{u}_{L,\pm}^{*\text{OBC}}(k) = \frac{1}{\sqrt{2h(h \mp h_z)}} \begin{pmatrix} h_x + i h_y \\ \pm h - h_z \end{pmatrix}, \quad (57)$$

also satisfy biorthogonal relations: $\underline{u}_{L,\alpha}^*(k) \cdot \underline{u}_{R,\alpha'}(k) = \delta_{\alpha,\alpha'}$. In presence of spectral mirror symmetry $\epsilon_{\pm}(k) = \epsilon_{\pm}(-k)$, left and right eigenvectors of H_{NH} in Eq. (41) can be constructed from a superposition of these non-Bloch waves at opposite momenta $\pm k$:

$$\begin{aligned} \underline{\psi}_{R,(\pm,k)}(j) &= \frac{r^j}{\sqrt{2N}} [e^{ikj} \underline{u}_{R,\pm}^{\text{OBC}}(k) - e^{-ikj} \underline{u}_{R,\pm}^{\text{OBC}}(-k)], \\ \underline{\psi}_{L,(\pm,k)}(j) &= \frac{(r^*)^{-j}}{\sqrt{2N}} [e^{ikj} \underline{u}_{L,\pm}^{\text{OBC}}(k) - e^{-ikj} \underline{u}_{L,\pm}^{\text{OBC}}(-k)], \end{aligned} \quad (58)$$

where j denotes the j -th unit cell with components on A and B sublattices encoded in \underline{u} . The relative minus sign in Eq. (58) reproduces the open boundary condition with one B site missing in the last unit cell:

$$\underline{\psi}_{R,(\pm,k)}(N) \Big|_B = \underline{\psi}_{L,(\pm,k)}(N) \Big|_B = 0, \quad \forall k. \quad (59)$$

It can be checked that both boundary and bulk eigenvectors respect biorthogonal relations in Eq. (44). Also, our exact solutions are valid for arbitrary parameters $t_1^{\pm}, t_2^{\pm} \in \mathbb{R}$ and arbitrary system size $2N - 1$.

To summarize, we obtain exact rapidity spectrum for a bosonic SSH chain in three dissipative setups of Eq. (41):

$$\begin{aligned} \beta_0 &= \begin{cases} \eta_1 + \eta_2, & \eta_0 \geq 0, \\ \eta_1 + \eta_2 + 2\eta_0, & \eta_0 < 0, \end{cases} \\ \beta_{\pm}(k) &= \eta_0 + \eta_1 + \eta_2 + i \epsilon_{\pm}(k), \quad \forall \eta_0, \end{aligned} \quad (60)$$

with $\epsilon_{\pm}(k)$ given by Eq. (56). The left and right boundary ($m = 0$) and bulk modes [$m = (\pm, k)$] of the damping matrix in Eq. (45) are constructed according to Eq. (46) and Eq. (58).

Bosonic reference steady state

In this section, we focus on the properties of solution C_s to the Lyapunov equation in Eq. (23). A general constraint imposed by the existence and uniqueness of C_s is obtained. Once satisfied, it leads to a unique BRSS. For our bond-dissipative model in absence of sublattice dissipation, singularities gather around the line of globally balanced gain and loss. Avoiding the singularities, solvable lines of C_s are identified where the BRSS has a simple uniform density profile, serving as a reference point to evaluate dynamical observables.

Existence of a unique BRSS and global-balance singular line

It is known that the solution Z to the Lyapunov equation in Eq. (22) exists and is unique if there is no pair of rapidities of the Liouvillian in Eq. (30) that renders $\beta_m + \beta_{m'} = 0, \forall m, m'$ [50]. In terms of the simplified Lyapunov equation in Eq. (23), we can show a similar constraint imposed on eigenvalues of NH damping matrix X . Let us apply the decomposition of $X = \sum_m \beta_m |\underline{\psi}_{Rm}\rangle\langle\underline{\psi}_{Lm}|$ to Eq. (23) and multiply from the left (right) side with $\langle\underline{\psi}_{Rm'}|(|\underline{\psi}_{Rm}\rangle)$. Due to the biorthogonal relations satisfied by eigenvectors $\underline{\psi}_{Lm}^* \cdot \underline{\psi}_{Rl} = \delta_{m,l}$, we obtain

$$(\beta_m + \beta_{m'}^*) \langle\underline{\psi}_{Rm'}|C_s|\underline{\psi}_{Rm}\rangle = \langle\underline{\psi}_{Rm'}|M^g|\underline{\psi}_{Rm}\rangle. \quad (61)$$

Combined with the identity $\mathbb{1}_{n \times n} = \sum_m |\underline{\psi}_{Rm}\rangle\langle\underline{\psi}_{Lm}|$, one arrives at a unique solution to C_s :

$$C_s = \sum_{m,m'} \frac{1}{(\beta_m + \beta_{m'}^*)} |\underline{\psi}_{Lm'}\rangle\langle\underline{\psi}_{Rm'}|M^g|\underline{\psi}_{Rm}\rangle\langle\underline{\psi}_{Lm}|, \quad (62)$$

given the condition

$$\beta_m + \beta_{m'}^* \neq 0, \quad \forall m, m'. \quad (63)$$

Under Eq. (63), the existence of a unique C_s [or equivalently, Z in Eq. (24)] also ensures that the bosonic Liouvillian is diagonalizable by our transformation matrix method in Eqs. (25)-(28).

Next, we show an important counterexample in our model of Eq. (36) where the BRSS captured by a unique C_s does not exist. It lies on the global-balance singular line without sublattice dissipation:

$$X = iH_S, \quad \text{at} \quad \eta_1 + \eta_2 = \frac{1}{2}(|\gamma_1^l| + |\gamma_2^l| - |\gamma_1^g| - |\gamma_2^g|) = 0, \quad |\gamma_0^l| = |\gamma_0^g| = 0. \quad (64)$$

Here, the total loss and gain on t_1 and t_2 bonds are equal. It turns out that in the eigenvalues of X given by $\beta_m = i\epsilon_m$, one can always find one pair of rapidities satisfying

$$\beta_m + \beta_{m'}^* = i(\epsilon_m - \epsilon_{m'}^*) = 0, \quad (65)$$

thus forbidding the existence of a unique C_s . For simplicity, we assume that the hopping parameters of H_S in Eq. (37) are all real: $t_i^\pm \in \mathbb{R}$. Combining this parity-time (PT) symmetry through complex conjugate operator K with generalized chiral symmetry represented by matrix $P = \text{diag}\{1, -1, 1, -1, \dots\}$:

$$[H_S, K] = 0, \quad PH_S P^{-1} = -H_S, \quad (66)$$

eigenvalues of H_S obey the condition: $\{\epsilon_m\} = -\{\epsilon_m\} = -\{\epsilon_m^*\} = \{\epsilon_m^*\}$. Meanwhile, the globally balanced gain and loss requires $M^g \neq 0$ in Eq. (37). For odd sites, from chiral symmetry one immediately identifies $E_0 = 0$ as one eigenvalue of H_S and Eq. (65) is satisfied at $m = m' = 0$. Since $0 \neq \langle\underline{\psi}_{R0}|M^g|\underline{\psi}_{R0}\rangle$ in Eq. (61), C_s has no solution. For even sites, from PT symmetry the eigenvalues of H_S either become real or form complex conjugate pairs: $m = m', \epsilon_m - \epsilon_{m'}^* = 0$ or $m \neq m', \epsilon_m - \epsilon_{m'}^* = 0$. Considering in both cases $0 \neq \langle\underline{\psi}_{Rm'}|M^g|\underline{\psi}_{Rm}\rangle$, a unique solution of C_s does not exist for even sites as well.

Solvable lines towards a uniform structure

Away from the global-balance singular line and in absence of sublattice dissipation:

$$\eta_1 + \eta_2 \neq 0, \quad \gamma_0^l = \gamma_0^g = 0, \quad (67)$$

one can find solvable lines of the Lyapunov equation in Eq. (23), along which the covariance matrix C_s holds a simple uniform structure:

$$C_s = a \cdot \mathbb{1}_{n \times n},$$

$$a = \frac{|\gamma_1^g| + |\gamma_2^g|}{|\gamma_1^l| - |\gamma_1^g| + |\gamma_2^l| - |\gamma_2^g|} = \frac{|\gamma_1^g|}{|\gamma_1^l| - |\gamma_1^g|} = \frac{|\gamma_2^g|}{|\gamma_2^l| - |\gamma_2^g|}. \quad (68)$$

Introducing variables

$$\eta = \eta_1 + \eta_2, \quad \eta_i = \frac{1}{2}(|\gamma_i^l| - |\gamma_i^g|),$$

$$\gamma = \gamma_1 + \gamma_2, \quad \gamma_i = \frac{1}{2}(|\gamma_i^l| + |\gamma_i^g|), \quad (69)$$

the solution of Eq. (68) exists once

$$\gamma_1 \gamma_2 = 0 \quad \text{or} \quad \frac{\gamma_1}{\eta_1} = \frac{\gamma_2}{\eta_2} \neq 0, \quad (70)$$

which renders a uniform density profile at the BRSS:

$$C_s = \left(\frac{\gamma - \eta}{2\eta} \right) \cdot \mathbb{1}_{n \times n}, \quad n_{\text{BRSS},j} = C_{s,jj} = \frac{\gamma - \eta}{2\eta}, \quad \text{at } \eta_0 = 0. \quad (71)$$

When elevating NH boundary mode with the sublattice dissipation, we are interested in two cases: the distillation scenario with loss on bonds and sublattice B ($\eta_0 > 0$), and the amplification scenario with gain on bonds and sublattice A ($\eta_0 < 0$). Satisfying $\gamma_1/\eta_1 = \gamma_2/\eta_2 = \pm 1$, they are also associated with a uniform covariance matrix:

$$C_s = \begin{cases} 0, & \eta_0 > 0; \\ -\mathbb{1}_{n \times n}, & \eta_0 < 0. \end{cases} \quad (72)$$

In the limit $\eta_0 \rightarrow 0$, C_s recovers the structure in Eq. (71) as for purely bond loss (gain), $\gamma = \eta$ ($-\eta$).

Stabilizing BRSS with a positive Liouvillian gap

We proceed to analyze the condition for a BRSS to become the steady state at large times. As shown in Fig. 5 (a), it requires a positive Liouvillian gap in the open system. For quadratic Lindbladians, the Liouvillian gap is defined from the lower bound of the real rapidity spectrum [28, 60]:

$$\Delta = 2 \min_{\forall m} \text{Re}[\beta_m]. \quad (73)$$

Different from fermions, the sign of bosonic Liouvillian gap can become negative. When $\Delta < 0$, from the diagonalized $\hat{\mathcal{L}}$ in Eq. (30), the density operator in the unbounded bosonic Liouville space keeps growing: $\rho_\infty = e^{\hat{\mathcal{L}}t} \rho_0|_{t \rightarrow \infty} \neq \rho_{\text{BRSS}}$, thus the system becomes unstable with $n_{t \rightarrow \infty, j} = \infty, \forall j$. Whereas, when $\Delta > 0$, the system relaxes to the BRSS at large times: $\rho_{\text{BRSS}} = e^{\hat{\mathcal{L}}t} \rho_0|_{t \rightarrow \infty}$ and $n_{t \rightarrow \infty, j} = n_{\text{BRSS}, j}, \forall j$. As a result, the bosonic Liouvillian gap is also referred to as the stability gap [51].

Without loss of generality, in Fig. 5 (a), we show the example of our model along the solvable lines of Eq. (70) where only bond loss and gain are present in the SSH chain. From the exact rapidity spectrum in Eq. (60) and Eq. (56), one obtains

$$\Delta = 2(\eta_1 + \eta_2) - 2 \sum_{i=1,2} \sqrt{\eta_i^2 - t_i^2} \cdot \theta(|\eta_i| - |t_i|), \quad \text{at } \eta_0 = 0, \quad (74)$$

where $\theta(x) = 1$, if $x > 0$ and $\theta(x) = 0$, otherwise. When the total bond loss is smaller than bond gain: $L = |\gamma_1^l| + |\gamma_2^l| < G = |\gamma_1^g| + |\gamma_2^g|$, or equivalently, $\eta = \eta_1 + \eta_2 < 0$, it results in $\Delta < 0$. There is no steady state and $n_{t \rightarrow \infty, j} = \infty, \forall j$. In fact, the uniform density of the BRSS in Eq. (71) depicted as blue curves in Fig. 5 (a) simultaneously turns negative: $n_{\text{BRSS}, j} < 0$. Once the total bond loss becomes larger than bond gain: $L > G$ or $\eta > 0$, the BRSS in Eq. (71) can

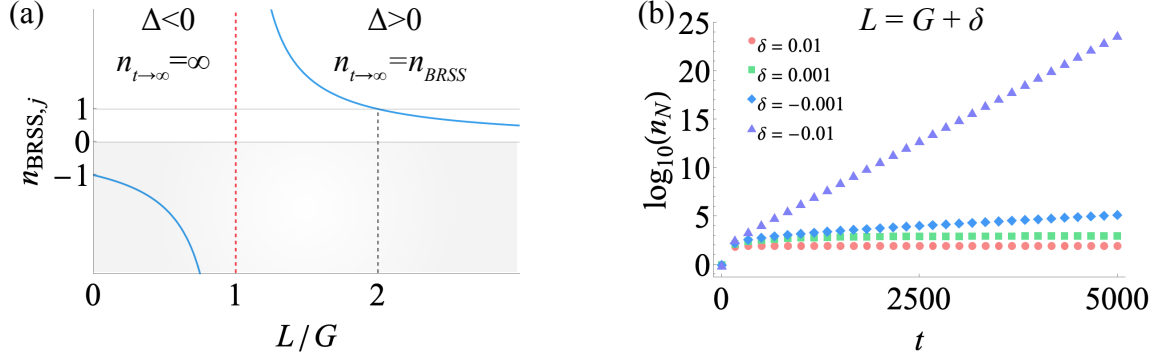


FIG. 5. **Stability of bosonic reference steady state.** We consider the solvable lines in Eq. (70) without sublattice dissipation $|\gamma_0^l| = |\gamma_0^g| = 0$. In (a), we show the particle density of a BRSS as a function of the rate between total bond loss and gain. In our notation, $L = |\gamma_1^l| + |\gamma_2^l|$, $G = |\gamma_1^g| + |\gamma_2^g|$. Given a positive Liouvillian gap $\Delta > 0$, the system can be stabilized to the BRSS at large times. Otherwise, the system becomes unstable with boson particle density diverging with time. (b) Particle density as a function of time approximating the global-balance singular line. We denote $L = G + \delta$ and take $t_1 = 1$, $t_2 = 2$, $\eta_1 = \frac{1}{2}\delta$, $\eta_2 = 0$ from $|\gamma_1^l| = |\gamma_1^g| + \delta = 1 + \delta$ and $|\gamma_2^l| = |\gamma_2^g| = 0$. We choose a system size $n_{\text{tot}} = 2N - 1 = 29$ and measure particle density at the middle of the chain: $n_j(t) = n_N(t)$. At $t = 0$, the system is prepared at a uniform distribution with one boson per site. As $\Delta = \delta \rightarrow 0^+$, the system relaxes to the BRSS with $n_{t \rightarrow \infty, j} = n_{\text{BRSS}, j} = G/\delta = 10^2, 10^3$ at $\delta = 0.01, 0.001$. As $\Delta = \delta \rightarrow 0^-$, we find $n_j(t) = c_0 e^{vt}$ at $t \gg 0$. By a fitting analysis in the time domain $t \in [2500, 5000]$, the exponential growth rate behaves as $v \simeq 0.0010288$ at $\delta = -0.001$, and $v \simeq 0.009998$ at $\delta = -0.01$, consistent with our prediction $v = |\delta|$ in Eq. (84).

be stabilized during relaxations if $\Delta > 0$. Taking into account both $\eta_1 + \eta_2 > 0$ and $\gamma_i > 0$, we deduce from Eq. (69) and Eq. (70) that $\eta_1 > 0, \eta_2 \geq 0$ or $\eta_1 \geq 0, \eta_2 > 0$. Combined with the analytical form of gap in Eq. (74), along the solvable lines $\Delta > 0$ is always satisfied when $L > G$. Given a positive Liouvillian gap, there exist several interesting limits shown in Fig. 5 (a). If only bond loss is present with $L > 0, G = 0$, the system relaxes to an empty chain: $n_{t \rightarrow \infty, j} = n_{\text{BRSS}, j} = 0, \forall j$. Meanwhile, since the Boson number in the Liouville space of Eq. (16) is unbounded from the upper side $\alpha_{\nu, j} \in \{0, 1, 2, 3, \dots\}$, to restrain the particle density $n_{t \rightarrow \infty, j} = n_{\text{BRSS}, j} \in [0, 1)$, it requires $L > 2G$. Otherwise, $n_{t \rightarrow \infty, j} = n_{\text{BRSS}, j} > 1$ for intermediate bond loss $G < L < 2G$. Additionally, $L = G$ denotes the global-balance singular line (red dashed) with no solution to a unique BRSS. Anomalous quantum dynamics close to the singular line will be studied in the next section.

It is useful to compare with quadratic fermionic Lindbladians. The fermionic Liouville space is bounded from both sides with an occupation number $\alpha_j \in \{0, 1\}$. From our earlier work [29], in the same bond dissipation setup the fermionic steady state (FSS) satisfies:

$$n_{\text{FSS}, j} = \frac{\gamma - \eta}{2\gamma} \in [0, 1], \quad (75)$$

where the Pauli principle is naturally respected. Under OBC, all the rapidities have positive real parts ensuring $\Delta > 0$. Therefore, the FSS can always be reached at large times regardless of relative strengths of bond loss and gain. In particular, with globally balanced gain and loss $L = G$ or $\eta = 0$, the steady state is at the half filling: $n_{\text{FSS}, j} = 1/2, \forall j$. Whereas, when the total bond loss is larger (smaller) than gain $\eta > 0$ ($\eta < 0$), the Fermi density of the FSS is below (above) the half filling.

Dynamical observables with uniform BRSS

It is straightforward to resolve the correlation matrix in Eq. (40) with the covariance matrix C_s of our uniform BRSS. Since $\partial_t C_s = 0$, after introducing $\tilde{C}(t) = C(t) - C_s$, the equation of motion can be recast into

$$\partial_t \tilde{C}(t) = -X^\dagger \tilde{C}(t) - \tilde{C}(t) X. \quad (76)$$

Starting from an initial state at $t = 0$, one arrives at $\tilde{C}(t) = e^{-X^\dagger t} \tilde{C}(0) e^{-Xt}$. Applying the decomposition of the damping matrix in Eq. (45), we get a compact form:

$$\tilde{C}_{jk}(t) = \sum_{m,m'} \sum_{l,l'=1}^{n_{\text{tot}}} e^{-(\beta_m + \beta_{m'}^*)t} \underline{\psi}_{Lm'}(j) \underline{\psi}_{Rm'}^*(l) \tilde{C}_{l,l'}(0) \underline{\psi}_{Rm}(l') \underline{\psi}_{Lm}^*(k), \quad (77)$$

where m and m' denote the band index. It is noted that any higher order correlator can be derived from this two-point correlator $C(t) = \tilde{C}(t) + C_s$ using the Wick theorem [50]. It is due to the fact that our uniform BRSS described by covariance matrix $C_{\text{BRSS}} = C_s$ in Eq. (71) and Eq. (72) is a Gaussian ground state of the quadratic Liouvillian in Eq. (30).

Going back to our three dissipation settings in Eq. (41), one can choose a convenient initial state for each. In the distillation case ($\eta_0 > 0$) with $C_s = 0$, we begin with a uniformly filled chain with x bosons per site ($x \geq 0$): $C(0) = x \times \mathbb{1}_{n \times n}$. The particle density evolution $n_j(t) = C_{jj}(t)$ follows

$$n_j(t) = x \times \sum_{m,m'} \sum_{l=1}^{n_{\text{tot}}} e^{-(\beta_m + \beta_{m'}^*)t} \underline{\psi}_{Lm'}(j) \underline{\psi}_{Rm'}^*(l) \underline{\psi}_{Rm}(l) \underline{\psi}_{Lm}^*(j). \quad (78)$$

In the amplification case ($\eta_0 < 0$) with $C_s = -\mathbb{1}_{n \times n}$, the same initial configuration $C(0) = x \times \mathbb{1}_{n \times n}$ leads to

$$n_j(t) = -1 + x \times \sum_{m,m'} \sum_{l=1}^{n_{\text{tot}}} e^{-(\beta_m + \beta_{m'}^*)t} \underline{\psi}_{Lm'}(j) \underline{\psi}_{Rm'}^*(l) \underline{\psi}_{Rm}(l) \underline{\psi}_{Lm}^*(j). \quad (79)$$

Example: dynamics approximating the global-balance singular line

Next, we study anomalous dynamics of an odd-length SSH chain close to the singular line in Eq. (64) where total bond gain and loss are in the balance. Associated with a uniform BRSS in Eq. (71), our solvable lines of Eq. (70) cross the singular line at $L = G$ or $\eta = \eta_1 + \eta_2 = 0$. In Fig. 5, we look at the two limits: $L = G + \delta$ with $\delta \rightarrow 0^\pm$. Choosing the initial state to be one boson per site $C(0) = \mathbb{1}_{n \times n}$, the particle density evolves as

$$n_j(t) = \frac{1}{\delta} \left[G + (\delta - G) \sum_{m,m'} \sum_{l=1}^{n_{\text{tot}}} e^{-(\beta_m + \beta_{m'}^*)t} \underline{\psi}_{Lm'}(j) \underline{\psi}_{Rm'}^*(l) \underline{\psi}_{Rm}(l) \underline{\psi}_{Lm}^*(j) \right], \quad (80)$$

with the rapidity spectrum and the Liouvillian gap ($|\eta_i| \ll |t_i|$)

$$\beta_0 = \frac{1}{2}\delta, \quad \beta_\pm(k) = \frac{1}{2}\delta + i\epsilon_\pm(k), \quad \Delta = \delta. \quad (81)$$

$\underline{\psi}_{R/L}$ and $\epsilon_\pm(k)$ are given by exact solutions in Eq. (46), Eq. (58) and Eq. (56) at $\eta_0 = 0$. Shown in Fig. 5 (b), when $\Delta = \delta \rightarrow 0^+$, as time passes the system evolves to the BRSS and becomes stabilized with uniform particle density:

$$n_{t \rightarrow \infty, j} = n_{\text{BRSS}, j} = \frac{G}{\delta}, \quad \forall j. \quad (82)$$

Whereas, when $\Delta = \delta \rightarrow 0^-$, the boson particle density continues to increase exponentially with time:

$$n_{t \rightarrow \infty, j} = c_0 e^{vt} \Big|_{t \rightarrow \infty} = \infty, \quad \forall j. \quad (83)$$

The exponential growth rate is estimated to be equal to the imbalance strength:

$$v \simeq -\Delta = |\delta|. \quad (84)$$

Liouvillian separation gap analysis

For an odd-length SSH chain under OBC, one can resolve analytically Liouvillian separation gap in the large N limit. By definition, $\Delta_s = \Delta_{\text{bulk}} - \Delta_{\text{boundary}}$ where the bulk and boundary Liouvillian gaps are derived from the

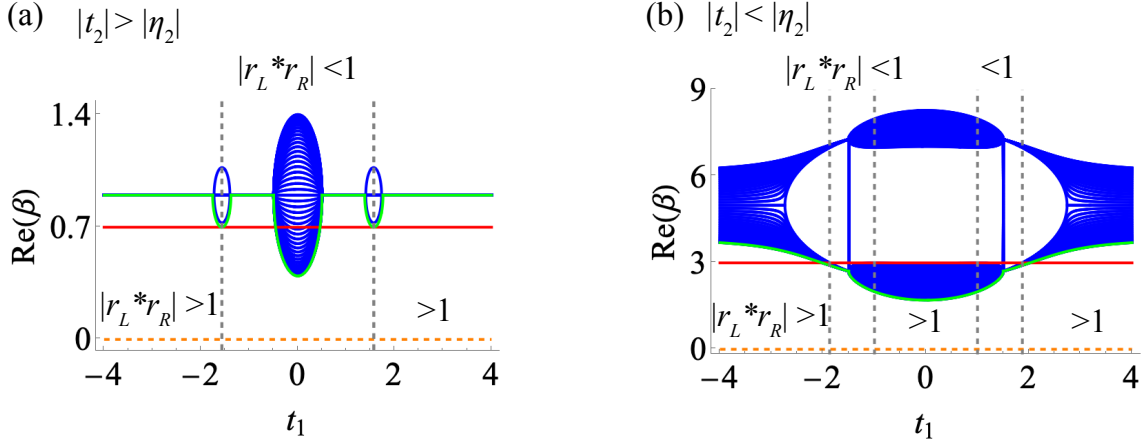


FIG. 6. **Bulk Liouvillian gap developed from the bottom of the real rapidity spectrum.** The green lines denote one half of bulk Liouvillian gap ($\Delta_{\text{bulk}}/2$) in the large N limit, analytically resolved in Eq. (87) by the relation $\Delta_{\text{bulk}} = \Delta_s + \Delta_{\text{boundary}}$. The blue lines show the real rapidity spectrum of bulk modes from exact solutions in Eq. (60) and Eq. (56) for a finite odd-length chain $n_{\text{tot}} = 2N - 1$ with $N = 46$. The boundary mode is depicted by red lines with a rapidity $\beta_0 = \eta_1 + \eta_2$, $\eta_0 > 0$. We fix $t_2 = 1.5$, $\eta_1 = 0.5$, $\eta_2 = 0.2$, $\eta_0 = 0.2$ in (a) and $t_2 = 1$, $\eta_1 = \eta_2 = 1.5$, $\eta_0 = 2$ in (b). In the chosen parameter region, the phase transitions occur at $|r_L^* r_R| = 1$, corresponding to $t_{1,c} = \pm\sqrt{t_2^2 - \eta_2^2 + \eta_1^2} \simeq \pm 1.568$ in (a) and $t_{1,c} = \pm\sqrt{\pm(t_2^2 - \eta_2^2) + \eta_1^2} \simeq \pm 1, \pm 1.871$ in (b).

rapidity spectrum in Eq. (60) and Eq. (56):

$$\Delta_{\text{boundary}} = \begin{cases} 2(\eta_1 + \eta_2), & \eta_0 \geq 0; \\ 2(\eta_1 + \eta_2) + 4\eta_0, & \eta_0 < 0, \end{cases}$$

$$\Delta_{\text{bulk}} = 2 \min_{k, \pm} \text{Re}[\beta_{\pm}(k)]. \quad (85)$$

We start with the first dissipative setting in Eq. (41) without sublattice loss or gain:

$$\eta_0 = 0, \quad \Delta_s = - \sum_{i=1,2} 2\sqrt{\eta_i^2 - t_i^2} \cdot \theta(|\eta_i| - |t_i|). \quad (86)$$

Apparently, for arbitrary $t_i, \eta_i \in \mathbb{R}$, $\Delta_s \leq 0$, indicating the boundary mode cannot become the single longest-lived mode in the relaxation process.

Next, we include the sublattice dissipation and look at our distillation ($\eta_0 > 0$) and amplification ($\eta_0 < 0$) schemes in Eq. (41). For $\eta_0 \neq 0$, the development of Liouvillian separation gap becomes a bit more involved. In the limit of large N , the discrete momentum for $\epsilon_{\pm}^{\text{OBC}}(k)$ in Eq. (50), $k = \pi \cdot m/N$ with $m = 1, 2, \dots, N-1$ can take the value close to $k = 0, \pi$. In Eq. (56), the extrema of $\epsilon_{\pm}^{\text{OBC}}(k)$ are then reached at $\cos(k) = \pm 1$. Differentiating the following three cases, we arrive at

$$\begin{aligned} \text{I. } |t_1| > |\eta_1| \text{ and } |t_2| > |\eta_2|, \\ \Delta_s &= 2|\eta_0| - 2\sqrt{\eta_0^2 - \left(\sqrt{t_1^2 - \eta_1^2} - \sqrt{t_2^2 - \eta_2^2}\right)^2} \cdot \theta(|\eta_0| - |\sqrt{t_1^2 - \eta_1^2} - \sqrt{t_2^2 - \eta_2^2}|); \\ \text{II. } |t_1| < |\eta_1| \text{ and } |t_2| > |\eta_2| \text{ or } |t_1| > |\eta_1| \text{ and } |t_2| < |\eta_2|, \\ \Delta_s &= 2|\eta_0| - \sqrt{2} \cdot \sqrt{\eta_0^2 + \eta_1^2 + \eta_2^2 - t_1^2 - t_2^2 + \sqrt{\eta_0^4 + 2\eta_0^2(\eta_1^2 + \eta_2^2 - t_1^2 - t_2^2) + (\eta_1^2 - t_1^2 + t_2^2 - \eta_2^2)^2}}; \\ \text{III. } |t_1| < |\eta_1| \text{ and } |t_2| < |\eta_2|, \\ \Delta_s &= 2|\eta_0| - 2\sqrt{\eta_0^2 + \left(\sqrt{\eta_1^2 - t_1^2} + \sqrt{\eta_2^2 - t_2^2}\right)^2}. \end{aligned} \quad (87)$$

Taking the limit $\eta_0 \rightarrow 0$ in each case, the initial setting without sublattice dissipation in Eq. (86) is retrieved. With finite η_0 , in Fig. 6 we check the validity of Eq. (87) in all three parameter regions by measuring bulk Liouvillian gap

$\Delta_{\text{bulk}} = \Delta_s + \Delta_{\text{boundary}}$ from the rapidity spectrum. Our prediction (green) for large system size N agrees well with exact solutions (blue) at $N = 46$. In particular, Fig. 6 (a) shows that for sufficiently large system size, at phase transitions $|r_L^* r_R| = 1$ the boundary mode enters the bulk rapidity spectrum, a feature which might be lost due to the finite-size gap in small systems, yet is accurately captured by our analytical result in the large N limit.

We are now ready to examine in each parameter region of Eq. (87) whether a positive Δ_s can be achieved by adding sublattice dissipation η_0 . If successful, NH boundary mode will be dynamically selected during relaxations.

It is noted that the critical points at phase transitions should be first excluded from the gap analysis:

$$|r_L^* r_R| = 1 \iff |t_1^2 - \eta_1^2| = |t_2^2 - \eta_2^2|. \quad (88)$$

It is when the bulk and boundary eigenmodes become degenerate, thus Δ_s is no longer well-defined. We will later recover the asymptotic behavior of $\Delta_s \rightarrow 0$ when approaching critical points.

$$\text{Region I: } |t_1| > |\eta_1|, |t_2| > |\eta_2|$$

When $|t_1| > |\eta_1|$ and $|t_2| > |\eta_2|$, one finds

$$\Delta_s > 0, \quad |\eta_0| > 0. \quad (89)$$

It is an ideal region where an infinitesimal η_0 can help select the boundary mode (see Fig. 2, blue curve). As $|\eta_0|$ slowly increases from zero, $\Delta_s = 2|\eta_0|$ keeps growing and the boundary mode becomes more and more predominant at large times. When $|\eta_0| > |\sqrt{t_1^2 - \eta_1^2} - \sqrt{t_2^2 - \eta_2^2}|$, Δ_s starts to decrease due to

$$\partial_{|\eta_0|} \Delta_s = 2 - \frac{2|\eta_0|}{\sqrt{\eta_0^2 - (\sqrt{t_1^2 - \eta_1^2} - \sqrt{t_2^2 - \eta_2^2})^2}} < 0. \quad (90)$$

Hence, we get an optimal η_0 to maximize Δ_s :

$$(\Delta_s)_{\text{max}} = 2|\sqrt{t_1^2 - \eta_1^2} - \sqrt{t_2^2 - \eta_2^2}|, \quad \text{at } |\eta_0|_{\text{opt}} = |\sqrt{t_1^2 - \eta_1^2} - \sqrt{t_2^2 - \eta_2^2}|. \quad (91)$$

Taking Fig. 1 (a)-(b) as an example, the optimal sublattice dissipation strength occurs at $\eta_0 \simeq (-)1.134$, generating the maximal Liouvillian separation gap between bulk and boundary modes in our (amplification) distillation protocol.

$$\text{Region II: } |t_1| < |\eta_1|, |t_2| > |\eta_2| \text{ or } |t_1| > |\eta_1|, |t_2| < |\eta_2|$$

When $|t_1| < |\eta_1|$ and $|t_2| > |\eta_2|$ or $|t_1| > |\eta_1|$ and $|t_2| < |\eta_2|$, we introduce two auxiliary functions to Eq. (87):

$$\begin{aligned} p &= \eta_1^2 + \eta_2^2 - t_1^2 - t_2^2, \quad q = \eta_1^2 - t_1^2 + t_2^2 - \eta_2^2, \\ \Delta_s &= 2\eta_0 - \sqrt{2} \cdot \sqrt{\eta_0^2 + p + \sqrt{\eta_0^4 + 2p\eta_0^2 + q^2}}. \end{aligned} \quad (92)$$

We can first eliminate the case $p > 0$, which renders $\Delta_s < 0$ (see Fig. 2, yellow curve). When $p < 0$, one identifies the gap closing point at

$$q^2 - p^2 + 4\eta_0^2 p = 0, \quad \Delta_s = 2|\eta_0| - \sqrt{2} \cdot \sqrt{\eta_0^2 + p + \eta_0^2 - p} = 0. \quad (93)$$

Moreover, for $0 < \eta_0^2 < (p^2 - q^2)/(4p)$, Δ_s increases monotonically with $|\eta_0|$:

$$\partial_{|\eta_0|} \Delta_s = 2 - \frac{\sqrt{2}|\eta_0|}{\sqrt{\eta_0^2 + p + \sqrt{\eta_0^4 + 2p\eta_0^2 + q^2}}} \left(1 + \frac{\eta_0^2 + p}{\sqrt{\eta_0^4 + 2p\eta_0^2 + q^2}}\right) > 1 - \frac{\eta_0^2 + p}{\eta_0^2 - p} > 0, \quad (94)$$

until it reaches zero at the gap closing point. Once $\eta_0^2 > (p^2 - q^2)/(4p)$, $\partial_{|\eta_0|} \Delta_s$ holds an upper non-negative bound:

$$\partial_{|\eta_0|} \Delta_s < 1 - \frac{\eta_0^2 + p}{\eta_0^2 - p}. \quad (95)$$

Taking the limit $|\eta_0| \rightarrow \infty$, one recognizes

$$\lim_{|\eta_0| \rightarrow \infty} \partial_{|\eta_0|} \Delta_s < 0, \quad \lim_{|\eta_0| \rightarrow \infty} \Delta_s = 0. \quad (96)$$

It indicates that Δ_s first increases to the maximal positive value, then decreases by further enlarging $|\eta_0|$. Also, Δ_s remains positive due to the lower bound at $|\eta_0| \rightarrow \infty$ (see Fig. 2, green curve). One thus arrives at the condition for a positive Δ_s in the second region:

$$\Delta_s > 0, \quad \text{if } \eta_1^2 + \eta_2^2 < t_1^2 + t_2^2 \text{ and } |\eta_0| > |\eta_0|_{\min} = \sqrt{(\eta_1^2 - t_1^2)(t_2^2 - \eta_2^2)/(t_1^2 + t_2^2 - \eta_1^2 - \eta_2^2)}. \quad (97)$$

The optimal η_0 is determined by a vanishing $\partial_{|\eta_0|} \Delta_s$. After a straightforward calculation, we identify

$$\partial_{|\eta_0|} \Delta_s = 0 \quad \Leftrightarrow \quad a\eta_0^6 + b\eta_0^4 + c\eta_0^2 + d = 0, \quad (98)$$

with $a = 4p, b = 9p^2 + 3q^2, c = 12pq^2$ and $d = 4q^4$. The task is simplified to finding the real roots of the cubic equation of η_0^2 . It leads to

$$(\Delta_s)_{\max} = \Delta_s(|\eta_0|_{\text{opt}}), \quad |\eta_0|_{\text{opt}} = \left[\frac{1}{4p} \left(h(p, q) - \frac{g(p, q)}{9h(p, q)} - 3p^2 - q^2 \right) \right]^{1/2}, \quad (99)$$

where the functions read

$$g(p, h) = -81p^2 + 90p^2q^2 - 9q^4, \\ h(g, h) = \left(-27p^6 + 45p^4q^2 - 17p^2q^4 - q^6 + 8\sqrt{p^6q^6 - 2p^4q^8 + p^2q^{10}} \right)^{1/3}. \quad (100)$$

$$\text{Region III: } |t_1| < |\eta_1|, |t_2| < |\eta_2|$$

When $|t_1| < |\eta_1|$ and $|t_2| < |\eta_2|$, it turns out that

$$\Delta_s < 0, \quad \forall \eta_0. \quad (101)$$

It is no longer possible to apply sublattice dissipation to elevate the boundary mode (see Fig. 2, red curve). Intuitively, as can be seen in Fig. 6 (b), in this region strong bond dissipation embeds the boundary mode too deep inside the real rapidity spectrum of bulk modes.

To summarize, we plot the development of Δ_s in the whole parameter range in Fig. 2. It shows the intricate interplay among the original Hamiltonian (t_1, t_2) and two different types of dissipation, the ones on bonds (η_1, η_2) and the other (η_0) on the sublattice. A positive Liouvillian separation gap can be achieved when $\eta_1^2 + \eta_2^2 < t_1^2 + t_2^2$ and $|\eta_0| > |\eta_0|_{\min}$. In this separable regime, we can also look at the critical behavior of Δ_s close to phase transitions $|t_1^2 - \eta_1^2| = |t_2^2 - \eta_2^2|$. In Region I, Eq. (91) infers $(\Delta_s)_{\max} = 2|\eta_0|_{\text{opt}} = 0$ at $t_1^2 - \eta_1^2 = t_2^2 - \eta_2^2$. In Region II, Eq. (97) leads to $|\eta_0|_{\min} = \infty$ at $t_1^2 - \eta_1^2 = -(t_2^2 - \eta_2^2)$. It indicates that the positive Δ_s would collapse to zero when approaching phase transitions, consistent with a degenerate bulk and boundary rapidity spectrum.

Polarization drift in an even-length chain

Aside from exact solutions to an odd-length chain, we provide numerical results on the non-solvable case of a chain with even length. Fig. 7 shows the behavior of the time-averaged polarization drift across topological phase transitions. Deep inside the topological region ($|r_L^* r_R| \ll 1$), D_p deviates from zero, indicating the emergence of a topological NH boundary mode exponentially localized on the sublattice A . Likewise, far away from the topological region ($|r_L^* r_R| \gg 1$), D_p vanishes completely consistent with the disappearance of any NH boundary mode. Near topological phase transitions ($|r_L^* r_R| = 1$), D_p fluctuates around zero. It originates from the finite-size effects in a small even-length system $n_{\text{tot}} = 2N = 30$. On one hand, the wavefunction of this topological boundary mode has a finite weight on the sublattice B with its lifetime reduced by the application of B -sublattice loss η_0 . On the other hand, its localization length r_ξ deviates from r_L , in contrast to the exact boundary mode in the odd-length chain of Eq. (46), which is valid for arbitrary system size $n_{\text{tot}} = 2N - 1$. Hence, a nonzero D_p does not arise precisely

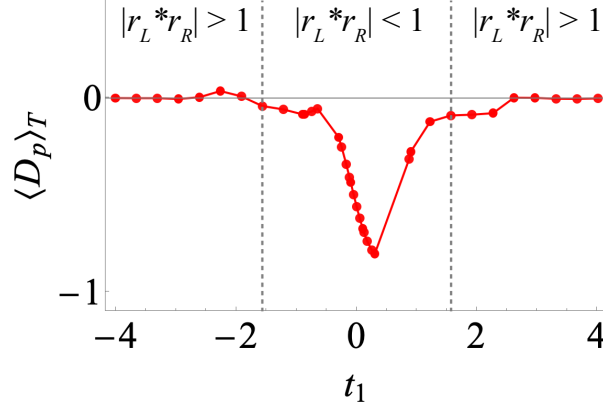


FIG. 7. **Even sites: finite polarization drift D_p driven by NH topological boundary mode.** We choose even sites $n_{\text{tot}} = 2N = 30$ at fixed $t_2 = 1.5$, $\eta_1 = 0.5$, $\eta_2 = 0.2$ with B -sublattice loss $\eta_0 = 1$. By varying t_1 , D_p deviates from zero deep inside the topological region $|r_L^* r_R| \ll 1$, elsewhere almost vanishes. For even sites, to reduce increased phase oscillations in polarization at large times, we perform a time-averaged measurement: $\langle D_p \rangle_T = (1/T) \sum_{k=0}^{T-1} D_p(t_{\text{max}} + k)$ with $t_{\text{max}} = 40$ and $T = 20$.

across $|r|^{-1} = |r_L|$ or $|r_L^* r_R| = 1$, obscuring its role as a topological marker for an even-length chain. With future improved algorithms and computational resources to diagonalize NH matrices, one may enlarge current system size and reduce these finite-size effects. However, it is possible that D_p may converge quickly to the behavior of $N \rightarrow \infty$ (purple dashed line in Fig. 4). Therefore, we do not recommend using D_p to predict topological phase transitions of an even-length chain. Nevertheless, D_p can be a good indicator of NH boundary mode deep inside the topological region.